Microbiology and Infectious Disease

Decoding the complexity of delayed wound healing following *Enterococcus faecalis* infection

Reviewed Preprint

Revised by authors after peer review.

About eLife's process

Reviewed preprint version 2
May 2, 2024 (this version)

Reviewed preprint version 1
March 13, 2024

Sent for peer review
January 10, 2024

Posted to preprint server
November 17, 2023

Cenk Celik, Stella Yue Ting Lee, Frederick Reinhart Tanoto, Mark Veleba, Kimberly A. Kline, Guillaume Thibault

School of Biological Sciences, Nanyang Technological University, Singapore • Singapore Centre for Environmental Life Science Engineering, Nanyang Technological University, Singapore • Department of Microbiology and Molecular Medicine, Faculty of Medicine, University of Geneva, Switzerland • Mechanobiology Institute, National University of Singapore, Singapore

Abstract

Wound infections are highly prevalent, and can lead to delayed or failed healing, causing significant morbidity and adverse economic impacts. These infections occur in various contexts, including diabetic foot ulcers, burns, and surgical sites. *Enterococcus faecalis* is often found in persistent non-healing wounds, but its contribution to chronic wounds remains understudied. To address this, we employed single-cell RNA sequencing (scRNA-seq) on infected wounds in comparison to uninfected wounds in a mouse model. Examining over 23,000 cells, we created a comprehensive single-cell atlas that captures the cellular and transcriptomic landscape of these wounds. Our analysis revealed unique transcriptional and metabolic alterations in infected wounds, elucidating the distinct molecular changes associated with bacterial infection compared to the normal wound healing process. We identified dysregulated keratinocyte and fibroblast transcriptomes in response to infection, jointly contributing to an anti-inflammatory environment. Notably, *E. faecalis* infection prompted a premature, incomplete epithelial-to-mesenchymal transition in keratinocytes. Additionally, *E. faecalis* infection modulated M2-like macrophage polarization by inhibiting pro-inflammatory resolution *in vitro*, *in vivo,* and in our scRNA-seq atlas. Furthermore, we discovered macrophage crosstalk with neutrophils, which regulates chemokine signaling pathways, while promoting anti-inflammatory interactions with endothelial cells. Overall, our findings offer new insights into the immunosuppressive role of *E. faecalis* in wound infections.

eLife assessment

Wounds are commonly infected, which can lead to delayed or poor wound healing, thereby significantly impacting morbidity and overall quality of life for patients. This manuscript uses single cell RNA sequencing to try to understand the impact of infection on various cell types during wound healing in a mouse model. The methodology is **solid** and the results provide a **valuable** 'atlas' of the cellular changes associated with infected and uninfected wounds which will be of interest to the field.

Introduction

Infections pose a challenge to the wound healing process, affecting both the skin's protective barrier and the efficient repair mechanisms required for tissue integrity. The skin, the largest and most intricate defense system in mammals, exhibits unique cellular heterogeneity and complexity that maintain tissue homeostasis. Within the skin, undifferentiated resident cells are the main modulators of tissue maintenance, albeit terminal differentiation dynamics adapt to the regenerative requirements of the tissue. Several comprehensive studies conducted in mice and humans have highlighted the complexity of the skin (Cheng et al., 2018; Der et al., 2019; Joost et al., 2020; Joost et al., 2018; Joost et al., 2016; Philippeos et al., 2018; Theocharidis et al., 2022). However, these studies have primarily focused on cellular heterogeneity and the transcriptome of intact skin or uninfected wounds, offering limited insights into the dynamics of wound healing following infection.

Efficient healing during wound infections involves a sequence of events occurring in three distinct but interconnected stages: inflammation, proliferation, and remodeling (Eming et al., 2014; Masson-Meyers et al., 2020; Minutti et al., 2017; Rognoni & Watt, 2018). These events involve a series of inter- and intracellular molecular interactions mediated by soluble ligands and the innate immune system (Lindley et al., 2016; Wang et al., 2018). The inflammatory phase initiates migration of leukocytes into the wound site to help clear cell debris and establish tissue protection through local inflammation. Initially, neutrophils, responding to pro-inflammatory cytokines like IL-1β, TNF-α, and IFN-γ, extravasate through the endothelium to the site of injury. Subsequently, the proliferative stage aims to reduce wound size through contraction and re-establishment of the epithelial barrier. This stage is facilitated by activated keratinocytes modulated by inflammatory responses, cytokines, and growth factors. In the final stage, tissue remodeling restores the mechanical properties of intact skin through ECM reorganization, degradation, and synthesis (Wang et al., 2018). Dysregulation of this intricate mechanism can lead to pathological outcomes characterized by persistent inflammation and excessive ECM production (Ashcroft et al., 2013).

Enterococcus faecalis (*E. faecalis*) is a commensal bacterium in the human gut, and also an opportunistic pathogen responsible for various infections, including surgical site infections and diabetic ulcers (Kao & Kline, 2019). Bacterial wound infections in general, including those associated with *E. faecalis,* are biofilm-associated, resulting in an antibiotic-tolerant population that may lead to persistent infections (Ch'ng et al., 2019). Additionally, *E. faecalis* has mechanisms to evade and suppress immune clearance by, for example, suppressing the pro-inflammatory M1-like phenotype in macrophage and preventing neutrophil extracellular trap formation (Kao et al., 2023; Kao & Kline, 2019; Tien et al., 2017). *E. faecalis* can also persist (Bertuccini et al., 2002; Gentry-Weeks et al., 1999; Horsley et al., 2018; Horsley et al., 2013; Olmsted et al., 1994; Wells et al., 1990; Wells et al., 1988; Zou & Shankar, 2014, 2016) and replicate (da Silva et al., 2022; Nunez et al., 2022) within epithelial cells and macrophages, further complicating treatment. The combination of biofilm formation and immune evasion makes Enterococcal wound infections a significant clinical challenge.

In a murine full-thickness excisional wound model, our prior investigations revealed a bifurcated trajectory characterizing *E. faecalis* wound infections (Chong et al., 2017). Initially, bacterial colony-forming units (CFU) increase in number in the acute replication phase, with a concomitant pro-inflammatory response characterized by pro-inflammatory cytokine and chemokine production coupled with neutrophil infiltration. In the subsequent persistence stage, *E. faecalis* CFU undergo gradual reduction and stabilization at approximately 105 CFU within wounds by 2-3-day post-infection (dpi), coinciding with delayed wound healing. Within this framework, we have identified specific bacterial determinants that contribute to each phase of *E. faecalis* infection. For

example, *de novo* purine biosynthesis emerges as a pivotal factor in enhancing bacterial fitness during the acute replication phase (Tan et al., 2022). In the persistent phase at 3 dpi, the galactose and mannose uptake systems, in conjunction with the *mprF* gene product, are associated with nutrient acquisition and resistance to antimicrobial peptides and neutrophil-mediated killing, respectively (Bao et al., 2012; Chong et al., 2017; Jin et al., 2021; Kandaswamy et al., 2013; Rashid et al., 2023). Nonetheless, the intricate interplay between these *E. faecalis* persistence-associated virulence factors, their immunomodulatory evasion strategies, and precise implications in the context of delayed wound healing remains to be investigated.

To address this, we generated a comprehensive single-cell atlas of the host response to persistent *E. faecalis* wound infection. We observed that *E. faecalis* induces immunosuppression in keratinocytes and fibroblasts, delaying the immune response. Notably, *E. faecalis* infection prompted a partial epithelial-to-mesenchymal transition (EMT) in keratinocytes. Moreover, macrophages in infected wounds displayed M2-like polarization. Our findings also indicate that the interactions between macrophages and endothelial cells contribute to the anti-inflammatory niche during infection. Furthermore, *E.* faecalis-infected macrophages drive pathogenic vascularization signatures in endothelial cells, resembling the tumor microenvironment in cancer. We also noted *E. faecalis* infected-associated macrophage crosstalk with neutrophils, regulating chemokine signaling pathways and promoting anti-inflammatory interactions with endothelial cells. These insights from our scRNA-seq atlas provide a foundation for future studies aimed at investigating bacterial factors contributing to wound pathogenesis and understanding the underlying mechanisms associated with delayed healing.

Results

E. faecalis infection inhibits wound healing signatures

In the wound environment, various cell types, including myeloid cells, fibroblasts, and endothelial cells, play critical roles in the initial and later stages of wound healing by releasing platelet-derived growth factor (PDGF). Additionally, macrophages secrete epidermal growth factor (EGF) in injured skin, which operates through the epidermal growth factor receptor (EGFR) to promote keratinocyte proliferation, migration, and re-epithelialization. To understand the impact of *E. faecalis* infection on wound healing, we infected excisional dorsal wounds on C57BL/6J male mice and measured gene expression levels of wound healing markers in bulk tissue at 4 dpi at the onset of persistent infection. We then compared the expression profiles with those of (i) wounded but uninfected or (ii) unwounded and uninfected controls, ensuring that the uninfected and infected mice were of comparable weight (**Figures 1A**, **S1A**, and **S1B**). We observed lower expression of platelet-derived growth factor subunit A (*Pdgfa*) in *E. faecalis*-infected wounds than in unwounded skin, while uninfected wounds remained unchanged. Similarly, the expression of *Egf* was lower in uninfected wounds than in healthy skin, while reaching the lowest levels in *E. faecalis*-infected wounds. The reduced *Egf* expression in uninfected wounds at 4 days post-wounding is expected, as EGF primarily influences skin cell growth, proliferation, and differentiation during the later stages of wound healing, typically around 10 days post-injury (Schultz et al., 1991). By contrast, wounding alone resulted in higher transforming growth factor beta 1 (*Tgfb1*) expression. TGF-β1 plays a dual role in wound healing depending on the microenvironment. During tissue maintenance, TGF-β1 acts as a growth inhibitor, and its absence in the epidermis leads to keratinocyte hyperproliferation (Guasch et al., 2007). Elevated TGF-β1 levels have also been observed in the epidermis of chronic wounds in both humans and mouse models (Li et al., 2021; Xie et al., 2009). In addition, we observed a slightly higher expression of fibroblast growth factor 1 (*Fgf1*) in uninfected wounds, although the differences were comparable (**Figure S1A**). Overall, the persistent *E. faecalis* infection contributed to higher *Tgfb1* expression, whilst *Pdgfa* levels remained low, correlating with delayed wound healing.

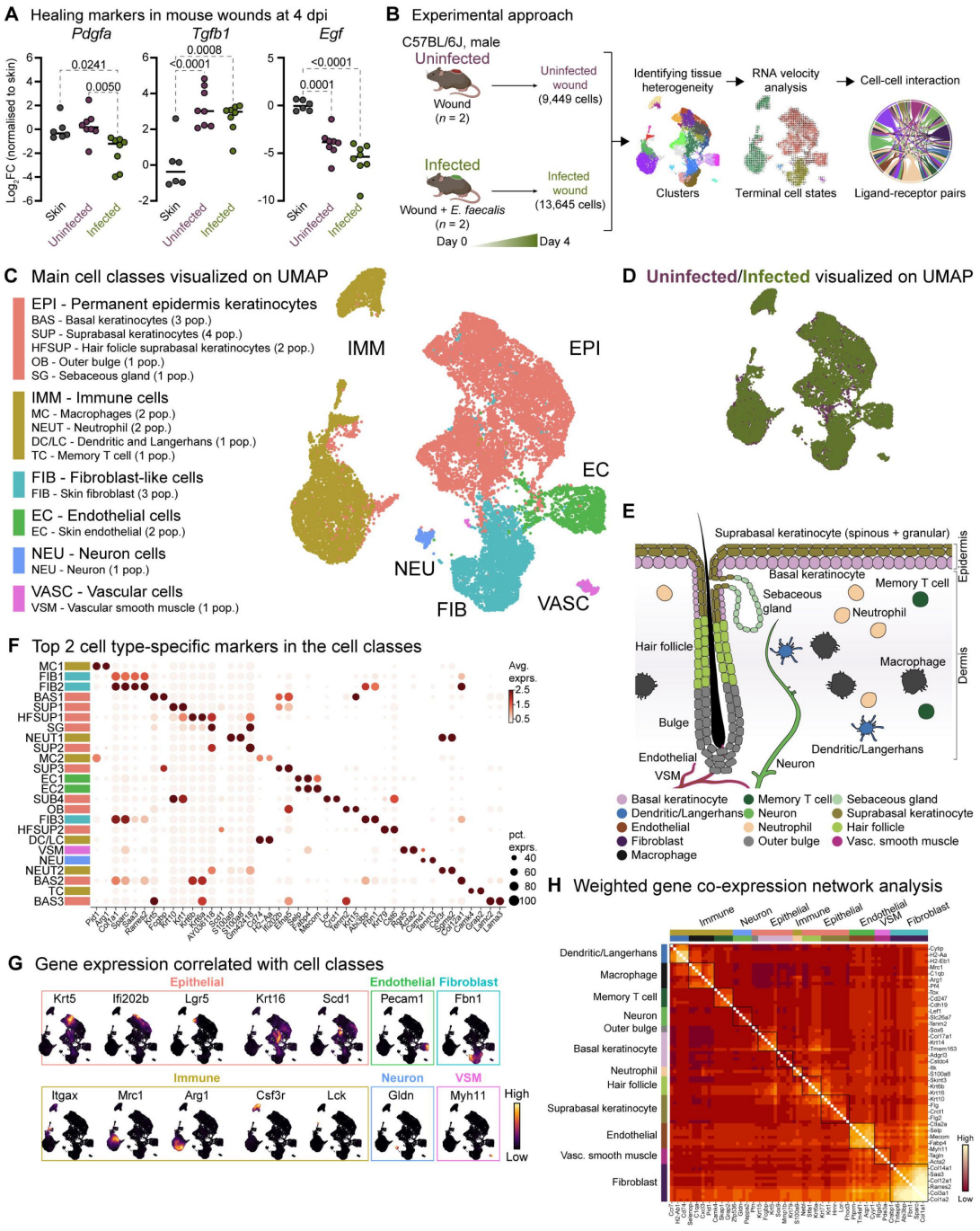

Figure 1.

Mouse skin wound infection atlas.

(A) Gene expression of healing markers *Pdgfa*, *Tgfb1* and *Egf* four days post-infection (4 dpi) for uninfected and *E. faecalis*-infected 6–7-week-old C57BL/6J mouse skin wounds, normalized to intact skin (n = 6 for skin; n = 8 for wounds; one-way ANOVA). **(B)** Single-cell RNA sequencing workflow of full-thickness mouse wounds. **(C)** Integrated dataset of ~23,000 scRNA-seq libraries from uninfected and infected wounds identifies 5 mega cell classes indicated in the UMAP. **(D)** UMAP colored by the uninfected and infected conditions. **(E)** Schematic describing the color-matched cell types with that of the clusters in Figure S1F. **(F)** Dot plot depicting the top two cell type-specific markers in the integrated data. Legend indicates average expression and dot size represents percent expression. **(G)** Density plots depict cell types described in C. **(H)** Heat map of weighted gene co-expression network analysis for annotated cell populations, colored by bars matching mega clusters and annotated cell types in C.

Single-cell transcriptomes of full-thickness skin wounds diverge during healing and infection

To understand the cellular heterogeneity in the wound environment following *E. faecalis* infection, we dissociated cells from full-thickness wounds, including minimal adjacent healthy skin. We generated single-cell transcriptome libraries using the droplet-based 10X Genomics Chromium microfluidic partitioning system (**Figure 1B** and **Table S1**). By integrating the transcriptomes of approximately 23,000 cells, we employed the unbiased graph-based Louvain algorithm to identify clusters (Zappia & Oshlack, 2018). Our analysis revealed 24 clusters, irrespective of infection (**Figure S1C**). These clusters included epithelial, immune, fibroblast, endothelial, vascular, and neural cell types (**Figures 1C, 1D**, **S1D**, **S1E**, and **Tables S2-S4**). Within the epithelial class, we identified basal (BAS1-3) and suprabasal (SUP1-4) keratinocytes, hair follicles (HFSUP1-2), outer bulge (OB), and sebaceous gland (SG) cells (**Figure 1E**). The immune class included macrophages (MC1-2), neutrophils (NEUT1-2), memory T cells (TC), and a mixed population (DC/LC) of dendritic cells (DCs) and Langerhans cells (LC). Notably, cells from infected wounds (~13,000 cells) demonstrated distinct clustering patterns compared to cells from uninfected wounds (~9,500 cells) (**Figure S1F** and **Table S1**).

We proceeded to analyze upregulated gene signatures for each Louvain cluster (**Figure 1F** and **Table S2**) and compared them to the cell-type signature database (Franzen et al., 2019) (PanglaoDB) to identify characteristic gene expression patterns (**Figure 1G**). Additionally, we identified highly expressed genes in uninfected and infected wounds (**Tables S3** and **S4**) and performed co-expression network analysis (WGCNA) to uncover the core genes associated with cell types (**Figure 1H**).

We also delineated macrophage populations (**Figure S1G-I**), identifying an M2-like polarization (**Figure 1F**, MC1) marked by higher expression of *Arg1*, *Egr2*, *Fn1*, and *Fpr2* (**Figure S1G**), and a tissue-resident macrophage (TRM) population (**Figure 1F**, MC2) expressing *Ccr5*, *Cd68*, *Fcgr1*, *Mrc1* (*Cd206*), *Ms4a4c*, and *Pparg* (**Figure S1H**). Both macrophage populations exhibited limited expression of *Grp18* and *Nos2* (*iNos*), which are typically associated with M1-like polarization (**Figure S1I**). Together, our analysis outlined the differences observed in uninfected and infected wound healing across epithelial, fibroblast, and immune cell populations.

E. faecalis elicit immunosuppressive interactions with keratinocytes

Keratinocytes, the predominant cell population in the skin, include undifferentiated (basal) and differentiated (suprabasal, hair follicle, outer bulge, and sebaceous gland) cells within the EPI cell class in both wound types (**Figure 1C**). Further analysis of the EPI class revealed 19 clusters (**Figure 2A** and **Table S5**), with the emergence of infection-specific clusters (**Figure 2B**, clusters 0 and 6, and **S2A**). We identified three major keratinocyte populations: (i) *Krt5*-expressing (*Krt5hi*) basal keratinocytes, (ii) *Krt10*-enriched (*Krt10hi*) post-mitotic keratinocytes, and (iii) *Krt5hiKrt10hi* co-expressing populations (**Figure 2C**). The co-expression of *Krt5* and *Krt10* was unique to infection-specific clusters (**Figure 2A**, clusters 0 and 6). We also observed distinct populations, including hair follicle stem cells (*Lrg5hi*; cluster 10), differentiating basal cells (*Ivlhi*; clusters 7 and 8), terminally differentiated keratinocytes (*Lorhi*; clusters 2, 8, 16, 17), and bulge stem cells (*Krt15hi*; clusters 2, 9, 10, 17, 18) (**Figure 2D**), reflecting the skin's complexity.

The two largest infection-specific clusters exhibited distinct gene expression patterns, with cluster 0 and cluster 6, enriched in *Zeb2* and *Gjb6* expression, respectively (**Figure 2A**). These clusters represent migratory stem-like and partial EMT keratinocyte populations (**Figure 2E**). As the barrier to pathogens, keratinocytes secrete a broad range of cytokines that can induce

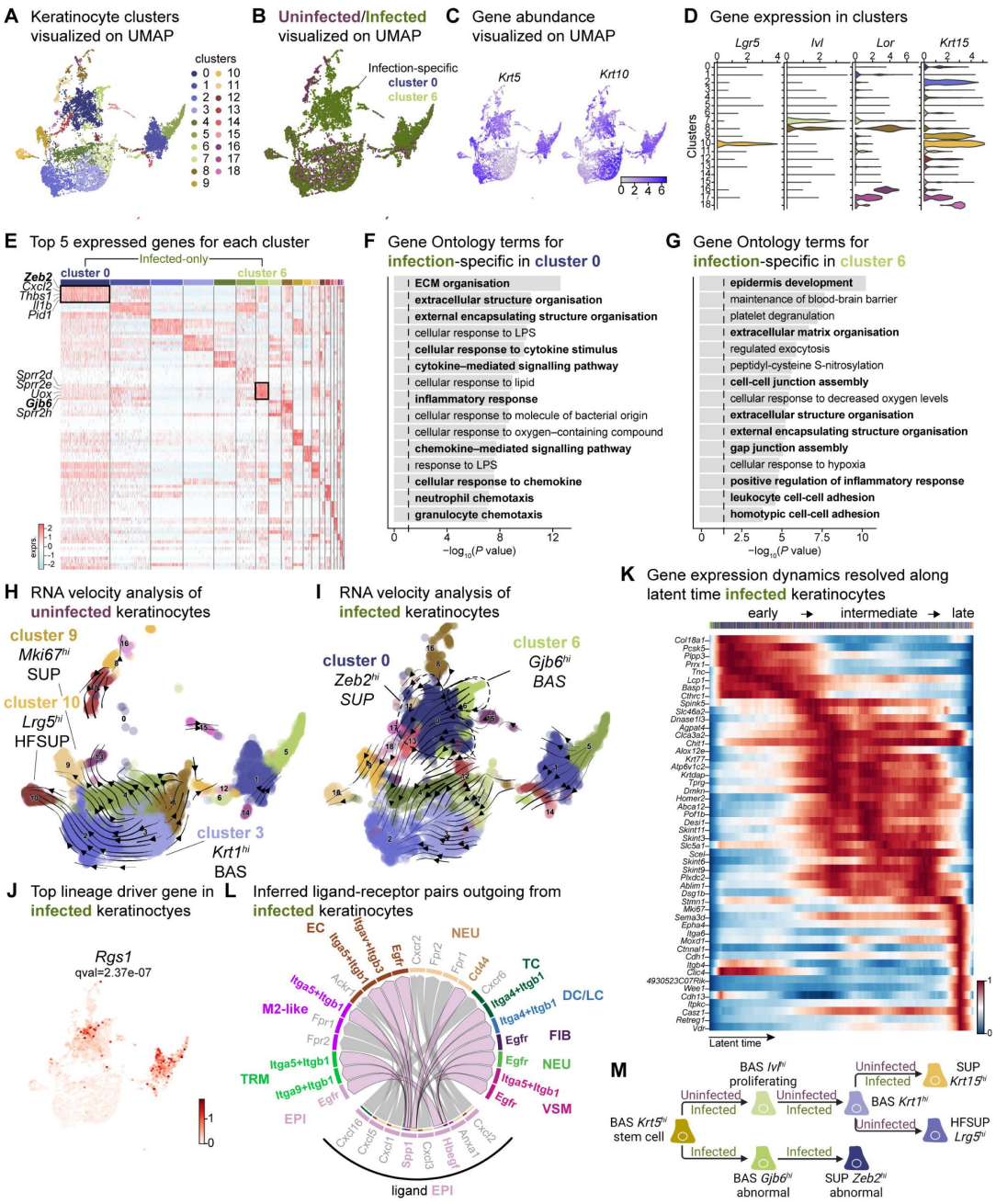

Figure 2.

Sub-clustering of keratinocyte populations reveals infection-specific cell types.

(A) UMAP of integrated keratinocyte (basal, suprabasal, hair follicle, bulge, and sebaceous gland) population reveals 19 clusters. **(B)** Infected keratinocytes (green) show unique and shared clusters with uninfected keratinocytes (purple). **(C)** Spatial dispersion of *Krt5* and *Krt10* abundance in keratinocytes. **(D)** Expression of *Lgr5*, *Ivl*, *Lor*, and *Krt15* in Louvain clusters shown in A. **(E)** Heat map of top 5 differentially expressed marker genes for each cluster in keratinocytes. Rectangle boxes indicate infection-specific Louvain clusters. **(F-G)** The bar plots show the top 15 Gene Ontology terms for infection-specific (F) *Zeb2hi* (cluster 0) and (G) *Gjb6hi* (cluster 6) keratinocyte populations. **(H-I)** Dynamic RNA velocity estimation of uninfected (H) and infected (I) keratinocytes. **(J)** The top lineage driver gene, *Rgs1*, in infected keratinocytes, was ubiquitously expressed in infection-specific Louvain clusters. (K) Gene expression dynamics resolved along latent time in the top 50 likelihood-ranked genes of infected keratinocytes. The colored bar at the top indicates Louvain clusters in I. Legend describes scaled gene expression. (L) Inferred ligand-receptor pairs outgoing from infected keratinocytes. (M) The hierarchy tree depicts the trajectory of differentiating and terminally differentiated keratinocyte cells originating from basal keratinocytes.

inflammatory responses (Alshetaiwi et al., 2020; Siriwach et al., 2022; Veglia et al., 2021). However, *Zeb2hi* keratinocytes co-expressing *Cxcl2*, *Il1b,* and *Wfdc17*, indicate myeloid-derived suppressor cell-like phenotype which implies an immunosuppressive environment (Hofer et al., 2021; Veglia et al., 2021). Gene Ontology analysis revealed that the *Zeb2hi* and *Gjb6hi* clusters exhibited signatures related to ECM remodeling, chemokine signaling, migratory pathways, and inflammatory response (**Figures 2F**, **2G**, and **Table S5**). Collectively, these findings suggest an early migratory role of keratinocytes induced by *E. faecalis* infection.

During cutaneous wound healing, keratinocytes enter a mesenchymal-like state, migrating to and proliferating within the wound site. We observed two infection-specific keratinocyte populations enriched in *Zeb2* and *Gjb6* expression, respectively, as early as four days post-wounding. To determine the nature of these populations, we performed RNA velocity analysis, a method that predicts the future state of individual cells based on the patterns of temporal gene expression (La Manno et al., 2018). RNA velocity analysis predicted a lineage relationship between *Zeb2hi* and *Gjb6hi* keratinocytes (**Figures 2H**, **2I**, and **Table S5**). The top lineage-driver genes (Lange et al., 2022), including *Rgs1*, *H2-Aa*, *Ms4a6c*, *Cd74*, *H2-Eb1* and *H2-Ab1*, were predominantly expressed in the infection-specific cluster 0 (**Figures 2J** and **S2B**). These genes are associated with the major histocompatibility complex (MHC) class II, suggesting a self-antigen presenting keratinocyte population, which have a role in co-stimulation of T cell responses (Meister et al., 2015; Tamoutounour et al., 2019). Meanwhile, *Gjb6hi* keratinocytes demonstrated reduced expression of putative genes such as *Pof1b*, *Krt77*, *Dnase1l3,* and *Krtdap* as well as increased *Clic4* expression (**Figure S2C**), suggesting that *E. faecalis* infection perturbs normal healing. Additionally, temporal expression analysis of high-likelihood genes revealed three distinct transcriptional states (**Figure 2K**): (1) an early state characterized by undifferentiated (basal) keratinocyte markers, (2) an intermediate state defined by the selection and upkeep of intraepithelial T cell protein family, and (3) a late state characterized by cell adhesion signatures. These findings provide insights into the cellular dynamics and developmental abnormalities, such as partial EMT induced by *E. faecalis* infection during wound healing.

Understanding cell-cell crosstalk through ligand-receptor interactions allows predicting ligand-target links between interacting cells by combining their expression data with signaling and gene regulatory network databases. Given our observation that infection-specific keratinocyte populations (**Figure S2**) were involved in ECM remodeling and immune response (**Figures 2F** and **2G**), we hypothesized that these cells might participate in the SPP1 signaling pathway. SPP1 (secreted phosphoprotein 1 or osteopontin) is a chemokine-like protein secreted by immune cells, osteoblasts, osteocytes, and epithelial cells to facilitate anti-apoptotic immune responses (Denhardt et al., 2001; Standal et al., 2004). To decipher ligand-receptor interactions in uninfected and infected skin wounds, we performed cell-cell interaction analysis (Guerrero-Juarez et al., 2019). We found 34 predicted interactions in uninfected keratinocytes and 61 in keratinocytes from *E. faecalis*-infected wounds out of a total of 923 and 991 interactions, respectively, in our single-cell atlas (**Figures S1A**, **S1B**, and **Table S6**). Importantly, we detected outgoing signals from keratinocytes to other cells associated with EGF and SPP1 signaling pathways. Ligand:receptor pairs in the infected niche (**Figure S2D**) included Hbegf:Egfr for the EGF pathway and Spp1:Cd44, Spp1:(Itga5+Itgb1), Spp1:(Itga9+Itgb1), and Spp1:(Itgav+Itgb3) for the SPP1 pathway (**Figures 2L**, **S2D**, and **S2E**), that are known to induce immunosuppression (Cheng et al., 2023; Gao et al., 2022). Remarkably, we observed the enrichment of keratinocyte-endothelial cell ligand:receptor pairs (**Figure S3** and **Table S6**). By contrast, keratinocytes from uninfected wounds only showed macrophage migration inhibitory factor (MIF) ligand interactions with its receptors Cd44, Cd74, and Cxcr4 in immune cells (DC/LC and TRM) (**Figure S2G**), suggesting that these keratinocytes promote cell proliferation, wound healing, and survival (Farr et al., 2020; Jager et al., 2020). Furthermore, the RNA velocity of keratinocytes from uninfected wounds revealed a terminal hair follicle (*Lrg5hi*) and a proliferating keratinocyte (*Mki67hi*) population originating from basal keratinocytes (**Figure 2H**), underlining normal wound healing. Overall, *E. faecalis* infection altered the transcriptome of keratinocytes towards a partial EMT at an early

stage, whereas uninfected keratinocytes showed differentiating and terminally differentiated keratinocyte populations (**Figure 2M**). Our data show that epidermal cells undergo migratory and inflammatory gene regulation during normal wound healing (Haensel et al., 2020; Vu et al., 2022), whereas *E. faecalis* induces anti-inflammatory transcriptional modulation that may promote chronicity in bacteria-infected skin wounds. These findings demonstrate that keratinocytes exist in a low inflammation profile under homeostasis, which is exacerbated upon *E. faecalis* infection.

E. faecalis delays immune response in fibroblasts

Fibroblasts are the fundamental connective tissue cells involved in skin homeostasis and healing. Upon injury, they primarily (1) migrate into the wound site, (2) produce ECM by secreting growth factors, and (3) regulate the inflammatory response. Despite their high heterogeneity, fibroblast subpopulations have distinct roles in wound healing. In response to injury, fibroblasts produce increased amounts of ECM by inhibiting the metalloproteinase (MMP) family through the tissue inhibitor of metalloproteinases 1 (TIMP1). Notably, Guerrero-Juarez *et al*. (2019) reported a rare fibroblast population expressing myeloid lineage cell markers during normal (uninfected) wound healing (Guerrero-Juarez et al., 2019). Our bioinformatic analysis identified fibroblast populations within wounds that differed significantly between infected and uninfected conditions (**Figure S1F**). Further analysis of the fibroblast mega class revealed 12 distinct clusters, with clusters 0 and 2 specific to infection while retaining their fibroblastic identity (**Figures 3A**, **3B**, and **Table S7**). The infection-associated fibroblasts express a range of markers, including those linked to extracellular matrix deposition such as *Col1a1*, *Col1a2*, *Col6a2*, vimentin (*Vim*), fibronectin, elastin (*Eln*), asporin (*Aspn*), platelet-derived growth factor receptor-beta (*Pdgfrb*), and fibroblast activator protein-α (*Fap*). These findings suggest a premature extracellular matrix deposition triggered by *E. faecalis*, which typically occurs in later stages of wound healing processes (Deng et al., 2021; Fang et al., 2023; Fitzgerald & Weiner, 2020) (**Figures 3C**, **3D**, **S4A**, and **S4B**).

The unique fibroblast clusters 0 and 2 associated with *E. faecalis* infection (**Figure 3E**) exhibited enrichment of myeloid-specific markers (*Hbb-bs*, *Lyz2*) and profibrotic gene signatures (*Inhba*, *Saa3*, *Timp1*) (**Table S6**). Additionally, *Lyz2hi* fibroblasts co-expressing *Tagln*, *Acta2*, and *Col12a1* suggested their origin as contractile myofibroblasts (Guerrero-Juarez et al., 2019). Gene Ontology analysis indicated that *Lyz2hi* fibroblasts were involved in immune response (**Figure 3F**), while *Timp1hi* fibroblasts were associated with tissue repair processes (**Figure 3G**). These findings collectively reveal an intricate cellular landscape within infected wounds, highlighting the detrimental functional contributions of various fibroblast subpopulations in response to *E. faecalis* infection.

To validate the distinct fibroblast cell states and their differentiation potential, we performed RNA velocity analysis (**Figures 3H** and **3I**), which revealed two terminal fibroblast populations: (1) a *Cilphi* fibrotic cluster 4 and (2) an *Mkxhi* reparative cluster 5, originating from clusters 0 and 2 (**Figure 3I** and **Table S7**), indicating the mesenchymal characteristics of infection-specific fibroblasts. Lineage driver gene analysis supported these findings, with the expression of genes such as *Csgalnact1*, *Atrnl1*, *Slit3*, *Rbms3*, and *Magi2*, which are known to induce fibrotic tissue formation under pathological conditions (Gornicki et al., 2022; Mizumoto et al., 2020) (**Figures 3J** and **S4C**). Similarly, the activation of genes such as *Serping1*, *Sparc*, *Pcsk5*, *Fgf7*, and *Cyp7b1* (**Figure S4D**) indicated the temporal activation of cell migration and immune suppression during infection. CellRank analysis revealed two states: an initial prolonged state and a short terminal state (**Figure 3K**). The early transcriptional states were associated with apoptosis inhibition, cell adhesion, and immune evasion genes, including serine protease inhibitors (*Serpine1* and *Serping1*), *Prrx1*, *Ncam1*, and *Chl1*, suggesting immune suppression. By contrast, the terminal state showed the emergence of migratory (*Cd74*, *Ifi202b*) and inflammatory (*Acod1*, *Cxcl2*, *F13a1*, and *S100a9*) genes, indicating a delayed immune response to *E. faecalis* infection. Overall, these findings indicate that uninfected fibroblasts contribute to healthy wound healing with

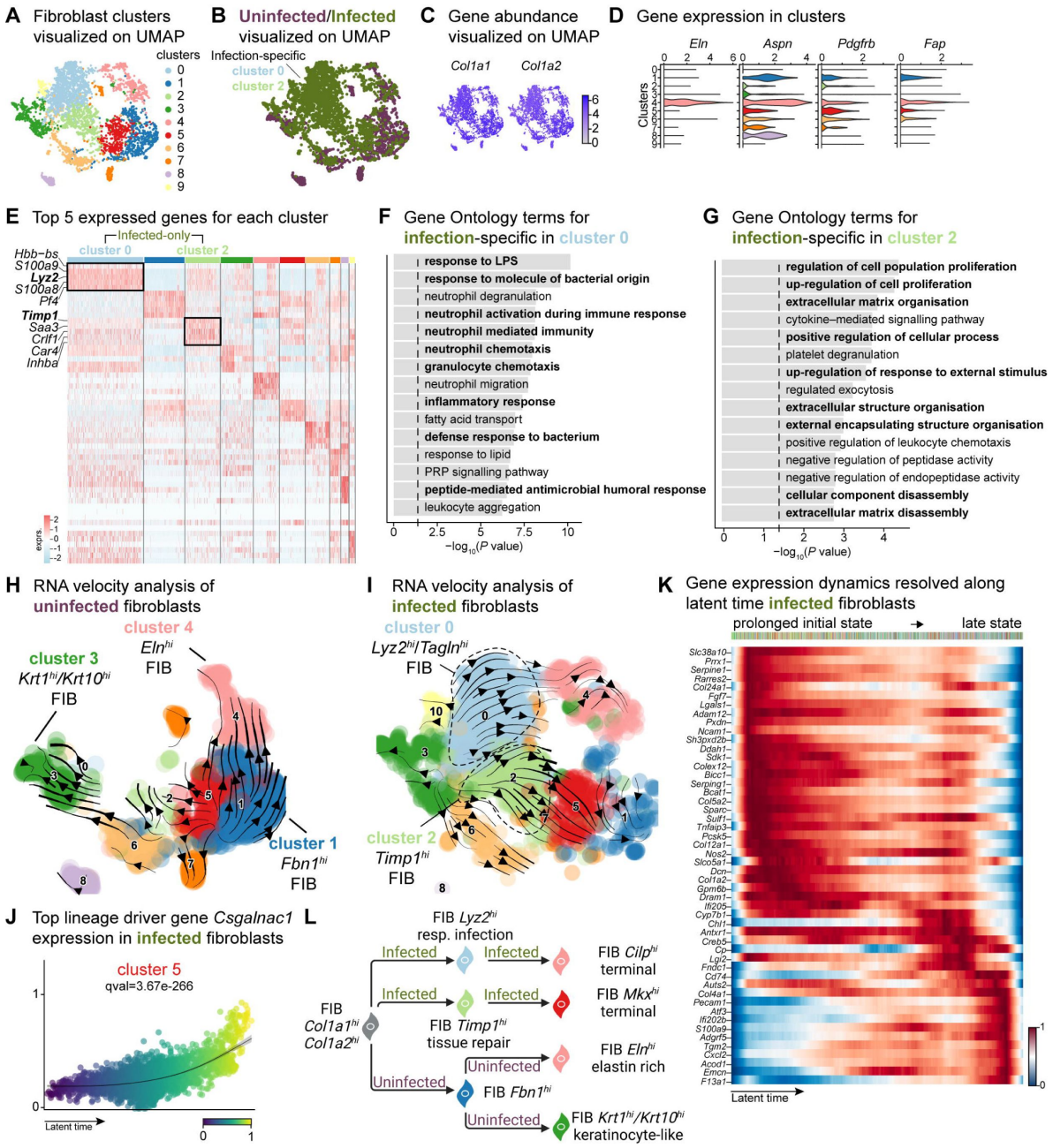

Figure 3.

E. faecalis delays immune response in fibroblasts.

(A) UMAP of integrated fibroblasts reveals 12 clusters. **(B)** Infected fibroblasts (green) show unique and shared clusters with uninfected fibroblasts (purple). **(C)** Spatial dispersion of *Col1a1* and *Col1a2* abundance in fibroblasts. **(D)** Expression of *Eln*, *Aspn*, *Pdgfrb* and *Fap* in Louvain clusters shown in A. **(E)** Heat map of top 5 differentially expressed marker genes for each cluster in fibroblasts. Rectangle boxes indicate infection-specific Louvain clusters. **(F-G)** The bar plots show the top 15 Gene Ontology terms for infection-specific (F) *Lyz2hi/Taglnhi* (cluster 0) and (G) *Timp1hi* (cluster 2) fibroblast populations. **(H-I)** Dynamic RNA velocity estimation of uninfected (H) and infected (I) fibroblasts. **(J)** The top lineage driver gene, *Csgalnac1*, expression in infected fibroblasts. **(K)** Gene expression dynamics resolved along latent time in the top 50 likelihood-ranked genes of infected fibroblasts. The colored bar at the top indicates Louvain clusters in I. Legend describes scaled gene expression. **(L)** While uninfected fibroblasts show healing phenotypes, infected fibroblasts undergo two transitioning phases: (i) contractile and (ii) pathologic.

proliferative and elastin-rich fibroblast populations. By contrast, *E. faecalis*-infected fibroblasts exhibit a pathological repair profile, characterized by the presence of *Timp1hi* and *Lyz2hi* fibroblasts (**Figure 3L**).

To understand the role of fibroblast subpopulations in healing, we explored cell-cell interactions in fibroblasts in infected wound (**Figure S4E**). In *E. faecalis*-infected wounds, we observed interactions involving Spp1 ligand with cell adhesion receptor Cd44 and integrins (Itgav+Itgb1, Itgav+Itgb3, Itgav+Itgb5, Itga4+Itgb1, Itga5+Itgb1, Itga9+Itgb1), and EGF signaling pairing Ereg:Egfr (**Figures S4F** and **S4G**). These interactions were particularly strong between macrophages (ligands) and endothelial cells (receptors) (**Figure S2C**), suggesting their involvement in the infected wound microenvironment. By contrast, uninfected wounds showed a normal wound healing profile with reparative VEGF and TGF-β signaling pathways (**Figures S4H** and **S4I**). Furthermore, RNA velocity analysis of fibroblasts from uninfected wounds revealed two terminal fibroblast populations originating from *Fbn1hi* fibroblasts: elastin-rich (*Elnhi*) fibroblasts and keratinocyte-like (*Krt1hi*/*Krt10hi*) fibroblasts (**Figure 3H**). Collectively, our findings revealed the unique roles of fibroblasts upon *E. faecalis* infection and reaffirmed the known functions of fibroblasts during uninfected wound healing, consistent with the outcomes of predicted ligand-receptor interactions (**Figure 3F**).

E. faecalis promotes macrophage polarization towards an anti-inflammatory phenotype

Immune cells play a crucial role in wound healing by eliminating pathogens, promoting keratinocyte and fibroblast activity, and resolving inflammation and tissue repair (Haensel et al., 2020; Landen et al., 2016; Vu et al., 2022). Our data reveal unique clusters enriched within keratinocytes and fibroblasts in *E. faecalis*-infected wounds, suggesting an immunosuppressive transcriptional program in these cell populations (**Figures S2A** and **S4B**). Given the ability of *E. faecalis* to actively suppress macrophage activation *in vitro* (Tien et al., 2017), we investigated if *E. faecalis* contributes to anti-inflammatory macrophage polarization and immune suppression *in vivo*. Analysis of the myeloid cells identified two infection-specific macrophage clusters (clusters 2 and 5) among 12 clusters (**Figures 4A, 4B**, and **Table S8**). To validate infection-specific macrophage polarization, we performed qPCR on bulk tissue isolated from uninfected and infected wounds at 4 dpi. Infected wounds showed downregulation of *Mrc1* and upregulation of both *Arg1* and *Nos2* compared to uninfected wounds or unwounded bulk skin tissue (**Figure 4D**), which was further corroborated by examining gene expression in bone marrow-derived macrophages (BMDM) following *E. faecalis* infection *in vitro* (**Figure 4E**). The co-expression of both M1-like and M2-like macrophage markers during infection has been previously reported for *M. tuberculosis* (Mattila et al., 2013), *T. cruzi* (Cuervo et al., 2011), and *G. lamblia* infections (Maloney et al., 2015), as an indicator of an immunosuppressive phenotype that promotes an anti-inflammatory environment during prolonged infection. In myeloid clusters of our scRNA-seq atlas, tissue-resident macrophages (*Mrc1*) were predominant in uninfected wounds, while M2-like macrophages (*Arg1*) were abundant in macrophages from *E. faecalis*-infected wounds (**Figures 4F** and **4G**), supporting the hypothesis of an anti-inflammatory wound environment during *E. faecalis* infection. Additionally, our analysis allowed the segregation of dendritic cells and Langerhans cells (cluster 10, *Cd207* and *Itgax*) from macrophage populations, characterized by the co-expression of langerin (*Cd207*) and integrin alpha X (*Itgax*/*Cd11c*) in cluster 10 (**Figure 4G**), confirming the validity of our cell annotation.

Next, we focused on the functions of infection-specific macrophage clusters 2 and 5 (**Figures 4B** and **S5B**) to identify their potential roles in wound infection. Gene Ontology analysis revealed that these macrophages were involved in the immune response, ECM production, and protein translation (**Figures S5C** and **S5D**). To better understand the evolution of infection-specific macrophages, we computed the RNA velocity to explore potential lineage relationships (**Figures 4H** and **4I**). RNA velocity identified cluster 2 macrophages as the terminal population in the

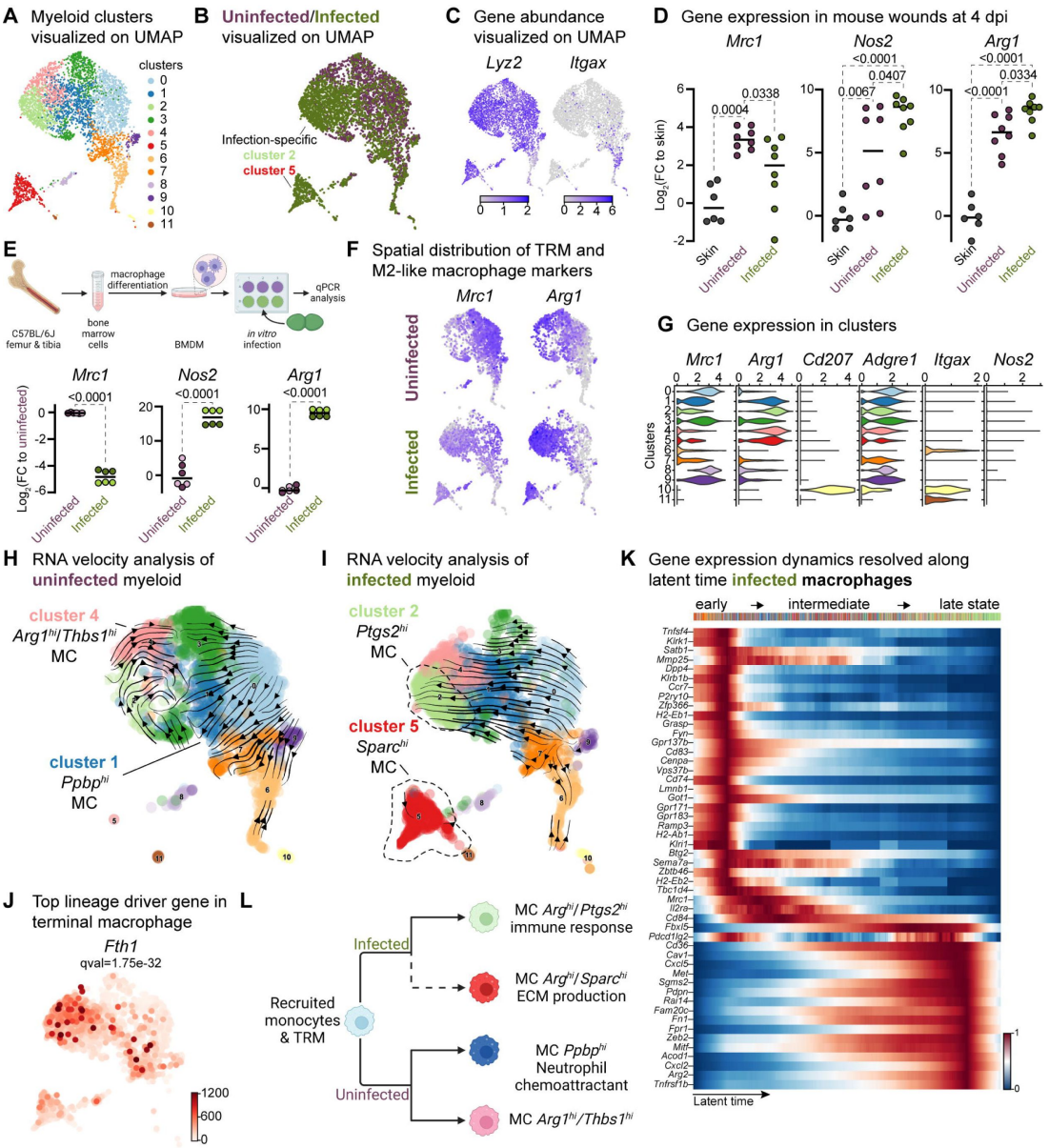

Figure 4.

Macrophages display M2-like polarization.

(A) UMAP of the integrated myeloid population reveals 9 macrophages, 2 dendritic cells, and one Langerhans cell cluster. **(B)** Infected myeloid (green) population show unique and shared clusters with the uninfected myeloid (purple) population. **(C)** Spatial distribution of *Lyz2* (macrophage) and *Itgax* (DC and LC) abundance in fibroblasts. **(D)** Gene expression *Mrc1*, *Nos2* and *Arg1* in mouse wounds at 4dpi, normalized to homeostatic skin (n = 6 for skin; n = 8 for wounds; one-way ANOVA). **(E)** *In vitro* infection of unpolarized (M0) bone marrow-derived murine macrophages (BMDMs) resulted in a down-regulation of TRM-associated marker *Mrc1* and an upregulation of M2-like markers *Nos2* and *Arg1*. Data are pooled from 2 biological replicates (shown in light and dark circles respectively) of 3 technical replicates each. **(F)** Spatial distribution of TRM and M2-like macrophage markers, *Mrc1* and *Arg1*, respectively. **(G)** Expression of *Mrc1*, *Adgre1*, *Arg1*, *Itgax*, *Cd207* and *Nos2* in the integrated myeloid dataset. **(H-I)** Dynamic RNA velocity estimation of uninfected (H) and infected (I) myeloid cells. **(J)** The top lineage driver gene, *Fth1*, was ubiquitously expressed in terminal macrophage populations. **(K)** Putative driver genes of infected macrophages. **(L)** The proposed model describes macrophage characteristics, where neutrophil-attracting and wound repair-associated macrophages were involved in uninfected wound healing. In contrast, bacteria-infected wounds are enriched in efferocytotic macrophages and matrix-producing macrophages.

infected dataset (**Figure 4I**), whereas uninfected terminal macrophage populations were found as clusters 1 and 4 (**Figure 4H**). As expected, cluster 5 did not exhibit velocity vectors since these cells were highly segregated from the main myeloid clusters and differed vastly in their gene expression (**Table S8**). While both terminal macrophage populations in both uninfected and infection conditions co-host anti-inflammatory macrophage signatures, their transcriptional program and functions vary in the presence of *E. faecalis* infection.

To further characterize clusters 2 and 5, we explored differentially expressed genes in infected cells. We identified the inflammation-related genes *Fth1*, *Slpi*, *Il1b*, *AA467197* (*Nmes1*/miR-147), *Ptges,* and *Cxcl3* (**Figures 4J** and **S5E**), suggesting that these cells may play a role in tissue remodeling (Munadziroh et al., 2022; Recalcati et al., 2019). Similarly, the expression of the infected-specific top likelihood genes *Cxcl2*, *Cd36,* and *Pdpn* was associated with the presence of efferocytic M2-like macrophages (**Figure S5F**, green clusters). The distant *Sparchi* macrophage cluster 5 exhibited C-C chemokine receptor type 7 (*Ccr7*) exhaustion (**Figure S5F**, red clusters), indicating that these cells might be of M1-like origin (Hu et al., 2020).

Next, to validate whether the terminal macrophage populations corresponding to clusters 2 and 5 were tissue-resident or M2-like macrophages, we computed the driver genes of macrophage sub-clusters over latent time. The top 50 likelihood gene heat map identified two major states in the macrophages (**Figure 4K**). The early state cells were enriched in antigen-presenting/processing MHC class II gene expression such as *H2-Ab1*, *H2-Eb1, H2-Eb2,* G-protein-coupled receptors (*Gpr137b*, *Grp171,* and *Gpr183*), and mannose receptor c-type 1 (*Mrc1*/*Cd206*). In contrast, *Cd36*, *Met*, *Sgms2*, *Fn1*, *Zeb2,* and *Arg2* levels were higher in the late macrophage population, suggesting M2-like polarization. Therefore, we asked whether these macrophages provide an immunosuppressive microenvironment during *E. faecalis* infection. Cellular interactome analysis revealed enrichment of the ANNEXIN signaling pathway, particularly Anxa1:Fpr1 and Anxa1:Fpr2 ligand-receptor pairs between M2-like macrophage and endothelial or neutrophil cells (**Figure S5I-K**), which inhibits pro-inflammatory cytokine production (Yang et al., 2009). Together, these results demonstrate that *E. faecalis* infection influences macrophage polarization towards an anti-inflammatory phenotype. Importantly, the ANXA1:FPR1 interaction has been implicated in the tumor microenvironment of several malignancies (Cheng et al., 2014; Takaoka et al., 2018; Vecchi et al., 2018; Zhao et al., 2022), indicating that the *E. faecalis*-infected wound niche mimics the anti-inflammatory transcriptional program of the tumor microenvironment.

Neutrophils contribute to the anti-inflammatory microenvironment

Our findings revealed an exacerbated inflammatory phenotype during infection (**Figures 2F**, **2G**, **3K**, and **4J**), specifically marked by an abundance of neutrophils (Chong et al., 2017) (**Figure 1D**). To facilitate a comparison of the broader immune niche, we focused on the neutrophil population, identifying six subpopulations in the integrated dataset (**Figure 5A** and **Table S9**). Among these, clusters 0 and 2 were abundant in the infected condition (**Figures 5B** and **S6A**). The expression of granulocyte colony-stimulating factor receptor (*Csf3r*) and integrin subunit alpha M (*Itgam*/*Cd11b*) was highly expressed across all neutrophils (**Figure 5C**). Furthermore, the higher expression of chemokine (CXC motif) receptor 2 (*Cxcr2*), Fc gamma receptor III (*Fcgr3*/*Cd16*), and ferritin heavy chain (*Fth1*) in clusters 0, 1, 2, 4 and 5 indicated the presence of migrating and maturing neutrophils, regardless of infection status (**Figure 5D**). By contrast, cluster 3 did not express *Cxcr2* and *Fcgr3* and had lower expression of *Fth1* but was enriched in calcium/calmodulin-dependent protein kinase type ID (*Camk1d*), suggesting that this neutrophil subpopulation recruited to the infected wound site might be mature but inactive (Chen et al., 2023; Evrard et al., 2018)

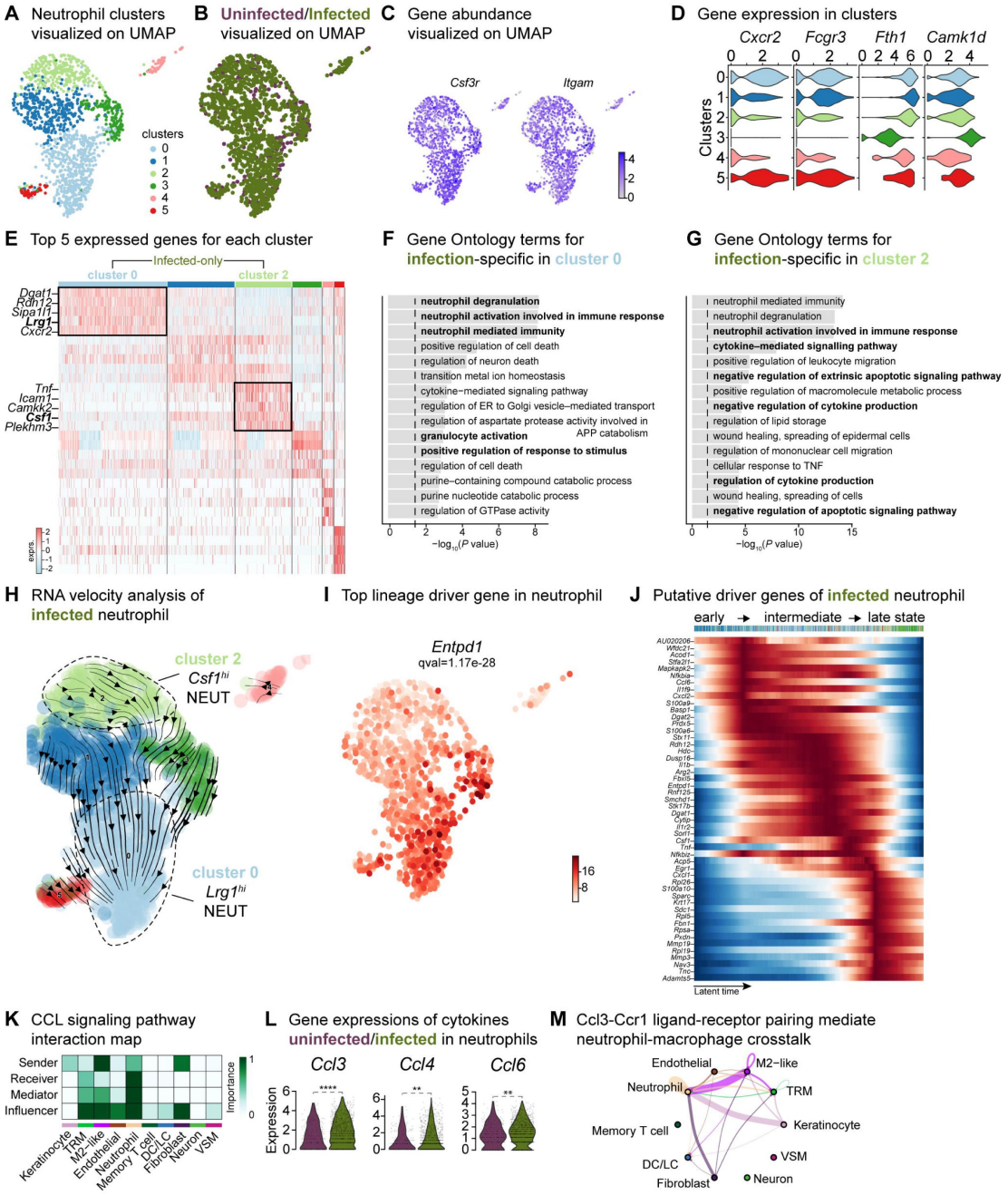

Figure 5.

Crosstalk between neutrophils and anti-inflammatory macrophages regulates the CCL signaling pathway.

(A) UMAP of the integrated myeloid population reveals 6 Louvain clusters. **(B)** The infected neutrophil (green) population shows unique and shared clusters with the uninfected neutrophil (purple) population. **(C)** Spatial organization of *Csf3r* and *Itgam* abundance in neutrophils. **(D)** Expression of *Cxcr2*, *Fcgr3*, *Fth1* and *Camk1d* in Louvain clusters. **(E)** Heat map of top 5 differentially expressed marker genes in neutrophils. Rectangle boxes indicate infection-specific Louvain clusters. **(F-G)** The bar plots show the top 15 Gene Ontology terms for infection-specific (F) *Lrg1*hi (cluster 0) and **(G)** *Csf1*hi (cluster 2) populations. **(H)** Dynamic RNA velocity estimation of infected neutrophils. **(I)** The top lineage driver gene, *Entpd1*, was ubiquitously expressed in *Lrg1*hi neutrophils (cluster 0). **(J)** Putative driver genes of infected neutrophil clusters. **(K)** Cytokine signaling pathway (CCL) cell-cell interaction map. **(L)** Gene expression of cytokines *Ccl3*, *Ccl4,* and *Ccl6* in neutrophils. **(M)** Ccl3:Ccr1 ligand-receptor interaction mediate neutrophil-macrophage crosstalk.

The infection-enriched neutrophils demonstrated a functional shift. Cluster 0 with higher expression of *Lrg1*, indicates an activated phagocytic phenotype (**Figure 5E-G**). By contrast, *Csf1hi* neutrophils (cluster 2) were associated with the negative regulation of apoptosis, cytokine production and neutrophil activation. *Csf1* upregulation in neutrophils mediates macrophage differentiation towards an immunotolerant phenotype (Braza et al., 2018), characterized by low expression of the lymphocyte antigen complex (LY6C) and increased proliferation rate. We then inspected the infected myeloid cells and observed a higher abundance of the cell proliferation marker, Ki-67 (*Mki67*), and the expression of lymphocyte antigen 6 complex locus 1 (*Ly6c1*). The expression of *Mki67* was specific to terminal macrophage population clusters 2 and 5 (**Figure S5G**) and the level of *Ly6c1* was lower in all macrophages but was specific to LCs (**Figure S5H**). These findings suggest that neutrophils may contribute to the anti-inflammatory polarization of *E. faecalis* infected macrophages.

RNA velocity analysis also estimated infected neutrophils with a propensity to become *Lrg1*hi neutrophils (**Figure 5H**, cluster 0), driven by genes *Entpd1*/*Cd39*, *Picalm*, *Hdc*, *Cytip*, *Sipa1l1* and *Fos* (**Figures 5I**, **S6B** and **S6C**). Moreover, suppression of *Nfkbia* and chemokine ligand-2 (*Cxcl2*) and upregulation of calprotectin (*S100a9*) together indicate an inflammatory response to *E. faecalis* infection (**Figure S6B**). To identify molecular changes that could drive neutrophil state transitions, we sorted the genes based on their peak in pseudo-time, revealing the three distinct neutrophil states: early-stage, intermediate-stage, and late-stage, in the *E. faecalis*-infected wounds (**Figure 5J**). The early response was characterized by *Ccl6*, *Il1f9* (*Il36g*), *Cxcl2*, *S100a6*, and *S100a9*, suggesting an initial pro-inflammatory neutrophil response. By contrast, the late stage demonstrated higher expression of ribosomal proteins (*Rpl5*, *Rpl19* and *Rpl26*), migratory metalloproteinases (*Mmp3*, *Mmp19* and *Adamts5*), and CXC motif ligand-1 (*Cxcl1*), suggesting perturbed neutrophil infiltration. MMP19 has also been implicated in M2 polarization (Fingleton, 2017), consistent with the anti-inflammatory signatures of the infected macrophage populations (**Figures 4J** and **S5E**). Cellular interactome analysis further predicted the anti-inflammatory status of neutrophils by a strong correlation in the CCL signaling pathway between neutrophils and M2-like macrophages, particularly through the Ccl3:Ccr1 axis (**Figures 5K-M** and **S6D**), an interaction predictive of neutrophil extravasation during *E. faecalis* infection (Hautz et al., 2023). Neutrophil extravasation is a vital event in immune responses to infections to ensure the survival of the host (Theocharidis et al., 2022). In summary, our single-cell analysis of neutrophils during *E. faecalis* wound infection revealed a perturbed pro-inflammatory resolution during infection that may contribute to anti-inflammatory macrophage polarization. Furthermore, our findings uncover prominent differences in immune cell composition in infected wounds, featuring *Lrg1*-rich neutrophil abundance (cluster 0), together with the enrichment of *Arg1hi* M2-like macrophage polarization (clusters 2 and 5). As such, wound healing during *E. faecalis* is characterized by a dysregulated immune response compared to uninfected wounds, which could be associated with delayed healing or chronic infection.

Anti-inflammatory macrophages induce pathogenic angiogenesis

Based on the role of angiogenesis in tissue repair, and our observations of the anti-inflammatory signatures provided by keratinocytes, fibroblasts, and macrophages, we investigated their impact on endothelial cells (ECs). First, we analyzed the two endothelial cell (EC) populations in the integrated dataset and identified 13 clusters with high *Pecam1* and *Plvap* expression. Notably, clusters 0 and 8 were exclusively found in the infected ECs. (**Figures 6A, 6B**, and **S7A-C**). These clusters were involved in ECM deposition, cell differentiation, and development, indicating an anti-inflammatory niche (**Figures 6C** and **6D**). Interestingly, RNA velocity analysis of infected ECs showed a faster velocity in the *Sparchi* (cluster 0) and *Cilphi* (cluster 8) cells, suggesting a dynamic transcriptional state (**Figure 6E**). The top lineage driver genes *Malat1*, *Tcf4*, *Rlcb1*, *Diaph2*, *Bmpr2*, and *Adamts9* indicate a pathogenic mechanism in proliferating ECs (**Figure 6F**).

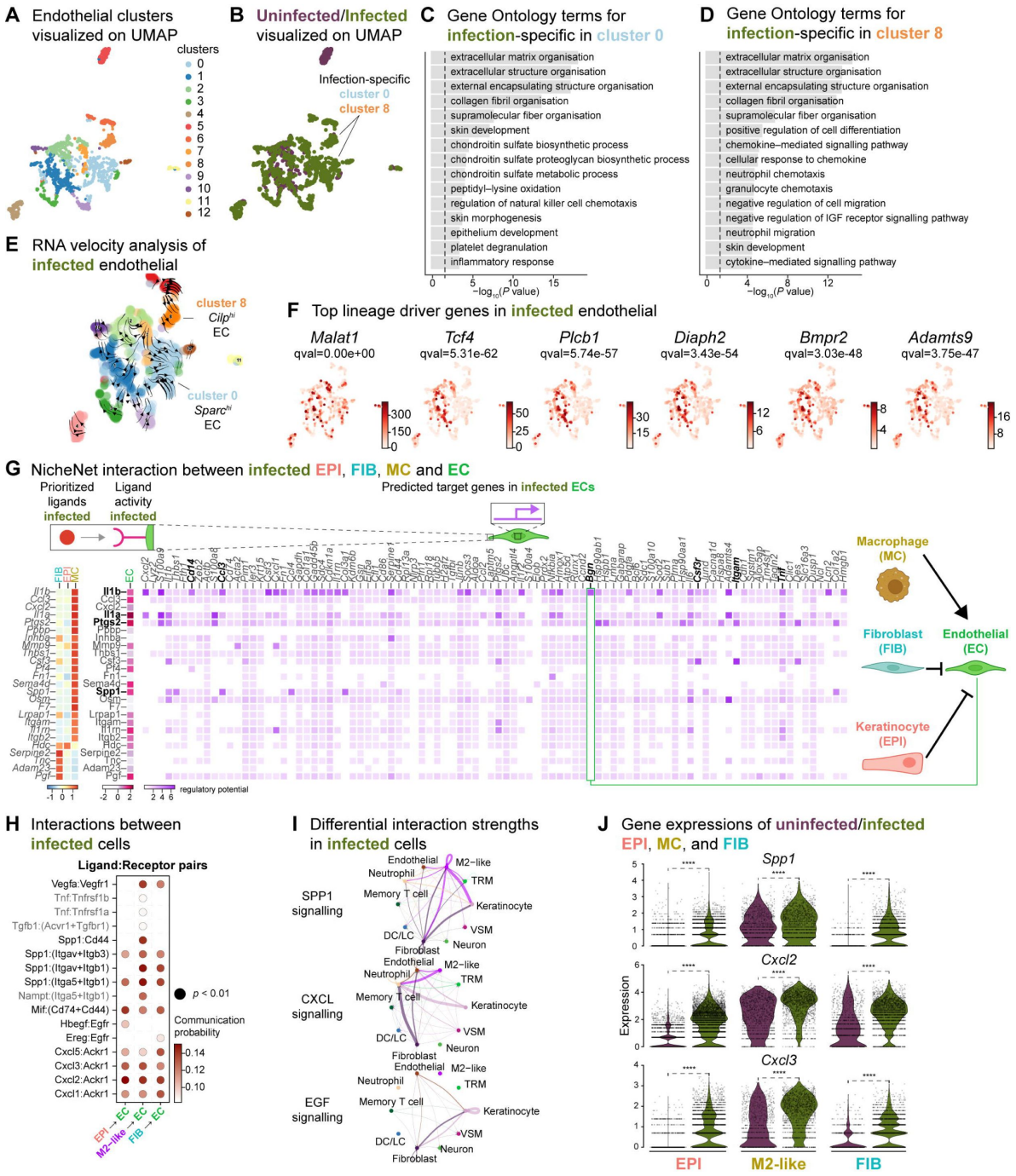

Figure 6.

Macrophage-EC interactions display an anti-inflammatory niche.

(A) UMAP of integrated endothelial cells reveals 13 clusters. **(B)** Infected endothelial cells (green) show unique and shared clusters with uninfected endothelial cells (purple). **(C-D)** Gene Ontology analysis of infection-specific clusters 0 (C) and 8 (D). **(E)** Dynamic RNA velocity estimation of infected endothelial cells. **(F)** The top lineage driver genes, *Malat1*, *Tcf4, Plcb1, Diaph2, Bmpr2,* and *Adamts9* in infected endothelial cells. **(G)** NicheNet interaction heat map between keratinocytes, fibroblasts, macrophages, and endothelial cells. Note the macrophage *Il1b*-specific *Bgn* induction in infected ECs. **(H)** The dot plot depicts interactions between endothelial cells (receptors) and keratinocytes, fibroblasts, and macrophages (ligands). Rows demonstrate a ligand-receptor pair for the indicated cell-cell interactions (column). **(I)** Differential interaction strengths of a cellular interactome for TNF, SPP1 and CXCL signaling pathways between all cell types in infection. **(J)** Spp1, Cxcl2, and Cxcl3 gene expression in keratinocytes, M2-like macrophages, and fibroblasts (Wilcoxon Rank Sum test, ****$p < 0.0001$).

We then explored whether the anti-inflammatory characteristics observed in infected epithelial cells, fibroblasts, and immune cells impacted ECs. To predict these cellular interactions, we conducted a differential NicheNet analysis (Browaeys et al., 2020), which involved linking the expression of ligands with corresponding receptors and downstream target gene expressions of these pairs in our scRNA-seq atlas of infected cells. Remarkably, NicheNet analysis revealed Il1b ligand of M2-like macrophages, correlated with the expression of target genes such as biglycan (*Bgn*), *Cd14*, *Ccl3*, *Csf3r*, *Itgam* and *Tnf* in ECs (**Figures 6G** and **S7D**), in line with previous studies (Perrault et al., 2018; Vu et al., 2022). Notably, BGN, a proteoglycan, has been associated with tumor EC signatures (Cong et al., 2021; Morimoto et al., 2021), further supporting the anti-inflammatory role of M2-like macrophages observed in the infected dataset. Moreover, the infection-induced expression of *Cd14* in EC suggests Toll-like receptor (TLR) activation (Dauphinee & Karsan, 2006; Lloyd & Kubes, 2006). Cell-cell interaction analysis also predicted that the Ptgs2, Spp1 and Il1a ligand activity in M2-like macrophages influenced the expression of target genes such as calprotectin (*S100a8* and *S100a9*) and colony-stimulating factor 3 (*Csf3*) These interactions suggest a potential disruption of EC integrity in the presence of *E. faecalis* infection. Similarly, according to the CellChat analysis, ECs exhibited activation of the SPP1 and CXCL signaling pathways (**Figures 6H-J**, **S7E** and **S7F**). Expression of the ligands Spp1, Cxcl2 and Cxcl3 were abundant in keratinocytes, fibroblasts, and M2-like macrophages during the infection (**Figure 6J**). In the uninfected ECs, however, fibroblasts modulated the expression of target genes such as TEK tyrosine kinase (*Tek*), Forkhead box protein O1 (*Foxo1*) and selectin-E (*Sele*), with notable angiopoietin 1 activity (**Figure S7D**), pointing to normal endothelial cell activity.

During unperturbed wound healing, macrophages modulate angiogenesis by producing proteases, including matrix metalloproteinases (MMPs), which help degrade the extracellular matrix in the wound bed. Additionally, macrophages secrete chemotactic factors such as TNF-α, VEGF and TGF-β to promote the EC migration (Du Cheyne et al., 2020; Wilkinson & Hardman, 2020). Furthermore, the TGF-β signaling pathway induces fibroblast proliferation and ECM production in wound healing (Cutroneo, 2007; Pakyari et al., 2013). Our analysis of the cellular interactome in the uninfected wound dataset revealed strong interactions in the TGF-β and VEGF signaling pathways (**Figure S7H-I**), corroborating previous studies (Joost et al., 2016; Vu et al., 2022). These findings suggest that uninfected wounds undergo reparative angiogenesis while *E. faecalis* infection evokes pathological vascularization. Overall, our analysis underlines the M2-like macrophage-EC interactions as targets of altered cell-cell signaling during bacteria-infected wound healing.

Discussion

Wound healing is an intricate process that involves the cooperation of various cellular and extracellular components. Disruptions to this network can perturb the healing dynamics. Previous scRNA-seq studies have primarily focused on the transcriptional profiles of epithelial and fibroblast populations in wound healing (Deng et al., 2021; Haensel et al., 2020; Joost et al., 2020; Joost et al., 2018; Joost et al., 2016). However, the impact of the host-pathogen interactions on wound healing transcriptional programs remains to be investigated. Here, our work presents the first comprehensive single-cell atlas of mouse skin wounds following infection, highlighting the transcriptional aberration in wound healing. *E. faecalis* has immunosuppressive activity in various tissues and infection sites (Chong et al., 2017; Kao et al., 2023; Kao & Kline, 2019; Tien et al., 2017). By surveying approximately 23,000 cells, we identified cell types, characterized shared and distinct transcriptional programs, and delineated terminal phenotypes and signaling pathways in homeostatic healing or bacterial wound infections. These scRNA-seq findings elucidate the immunosuppressive role of *E. faecalis* during wound infections, providing valuable insights into the underlying mechanisms.

To explore the cellular landscape of *E. faecalis*-infected wounds and the impact of infection on wound healing, we focused on cell types specifically enriched in these tissues. Our analysis revealed infection-activated transcriptional states in keratinocytes, fibroblasts, and immune cells. The presence of clusters 0 and 6, exclusive to the epithelial dataset, along with RNA velocity analysis pointing to *Zeb2*-expressing cells (**Figure 2I**), suggests a potential role of *E. faecalis* in promoting a partial EMT in keratinocytes. We also identified a terminal keratinocyte population (cluster 2) at 4 dpi, characterized by the consumption of *Krt77* and *Krtdap* over pseudo-time, confirming terminal keratinocyte differentiation (**Figures 2I and S2C**). By contrast, uninfected wounds showed proliferating keratinocyte (*Mki67hi*) and hair follicle (*Lrg5hi*) cells (**Figure 2H**), consistent with previous findings on wound healing and skin maintenance signatures (Joost et al., 2020; Joost et al., 2018). Furthermore, we found two infection-specific fibroblast populations enriched in *Lyz2*/*Tagln* and *Timp1*, identifying their myofibroblast characteristics. The RNA velocity analysis confirmed cluster 5 as the terminal fibroblast population derived from myofibroblasts (cluster 2) (**Figure 3I**). Additionally, an increase in *Timp1* expression correlated with cell growth and proliferation signatures (*Sparc*, *Fgf7* and *Malat1*) over latent time in cluster 5 (**Figures S4C and S4D**). These findings collectively demonstrate a profibrotic state in fibroblasts driven by *E. faecalis*-induced transcriptional dynamics.

To investigate the impact of immunosuppressive signatures in keratinocytes and fibroblasts, we examined how *E. faecalis* infection influenced the immune response in wounds. Given that prolonged macrophage survival is associated with impaired wound healing (Kim & Nair, 2019; Krzyszczyk et al., 2018), we primarily focused on the macrophage populations. We identified subpopulations of M2-like macrophages expressing *Arg1*, *Ptgs2* and *Sparc* genes (**Figure 4F-I**). COX-2 (cyclooxygenase-2, encoded by *Ptgs2* gene) has been reported as a crucial regulator of M2-like polarization in tumor-associated macrophages (Na et al., 2013; Wang et al., 2021). While macrophage polarization is complex in humans and other higher organisms (Orecchioni et al., 2019; Watanabe et al., 2019), our scRNA-seq data suggests that *E. faecalis* infection drives an anti-inflammatory microenvironment resembling the tumor microenvironment. These findings confirm and expand on previous studies highlighting the immunosuppressive role of *E. faecalis* in different contexts (Chong et al., 2017; Kao & Kline, 2019; Tien et al., 2017).

Our findings also elaborate on the potential cell-cell communication and signaling pathways involved in wound healing. Ligand-receptor interaction analysis revealed an immune-suppressive ecosystem driven by M2-like macrophages during bacterial infection (**Figure 6G**). CellChat analysis confirmed that M2-like macrophages play a crucial role in regulating angiogenesis through the Vegfa:Vegfr1 ligand-receptor pair (**Figures 6H**, **6I**, **S7E**, **S7F**, and **Table S6**). Further, the Spp1 ligand correlated with integrins (Itgav+Itgb1, Itgav+Itgb3, Itga5+Itgb1) and the cluster of differentiation receptor Cd44 in ECs. Notably, while the Spp1 ligand of macrophages registered strong interactions with ECs, infected keratinocytes and fibroblasts were identified as the primary sources of Spp1 ligand. The infection-specific abundance of *Spp1* in these clusters highlight a partial EMT state in our extended analyses (**Figures 2E-I**). Furthermore, the interaction between Spp1 and Cd44 in M2-like macrophages and ECs indicated a proliferative state. The neutrophil chemokine *Cxcl2*, which promotes wound healing and angiogenesis (Girbl et al., 2018; Sawant et al., 2021), strongly correlated with the atypical chemokine receptor *Ackr1*, suggesting neutrophil extravasation. Additionally, the secretion of heparin-binding epidermal growth factor (*Hbegf*) by keratinocytes and epiregulin-enriched fibroblasts (*Ereghi*) further confirmed the presence of an anti-inflammatory microenvironment and angiogenic ECs in bacteria-infected wounds (**Figures 6H**, **6I**, and **S7F**).

In summary, our study provides insights into the cellular landscape, transcriptional programs, and signaling pathways associated with uninfected and *E. faecalis*-infected skin wounds. We confirm the immune-suppressive role of *E. faecalis* in wound healing, consistent with previous findings in different experimental settings (Chong et al., 2017; Kao et al., 2023; Tien et al., 2017 Kao, 2023 #134). Importantly, we identify specific ligand-receptor pairs and signaling pathways affected

during wound infection. The increased number of predicted signaling interactions suggests that *E. faecalis* modulates cellular communication to alter the immune response. Notably, the CXCL/SPP1 signaling pathway emerges as a critical player in shaping the immune-altering ecosystem during wound healing, highlighting its potential as a therapeutic target for chronic infections. Collectively, our findings demonstrate the collaborative role of keratinocytes, fibroblasts, and immune cells in immune suppression through CXCL/SPP1 signaling, providing new avenues for the treatment of chronic wound infections.

Limitations of the study

Our study provides a comprehensive comparison of the transcriptomic and cellular communication profiles between uninfected and *E. faecalis*-infected full-thickness mouse skin wounds at four days post-infection. However, our study lacks a reference dataset of uninfected, unwounded dorsal skin transcriptome, which would have allowed us to investigate transcriptomic changes temporally, especially induced by the wounding alone. Although we explored public datasets to address this limitation (Haensel et al., 2020; Vu et al., 2022), the low number of cells in public datasets, particularly for macrophage populations (data not shown), prevented their inclusion in our analysis. Additionally, the absence of multiple time points hinders our ability to examine temporal changes and the dynamic kinetics of host responses following infection.

Methods

Arg1	CAG AAG AAT GGA AGA GTC AG	CAG ATA TGC AGG GAG TCA CC
Egf	TGG CTC GAA GTC AGA TCC ACA	TTC TCG GGC ACA TGG TTA ATG
Gapdh	TCA GGA GAG TGT TTC CTC GTC CC	TCT CGG CCT TGA CTG TGC CG
Fgf1	CCC TGA CCG AGA GGT TCA AC	GTC CCT TGT CCC ATC CAC G
Mrc1	TTC AGC TAT TGG ACG CGA GG	GAA TCT GAC ACC CAG CGG AA
Nos2	TGT CGC AGC TCC CTA TCT TG	GGA AGC CAC TGA CAC TTC GC
Pdgfa	TGG CTC GAA GTC AGA TCC ACA	TTC TCG GGC ACA TGG TTA ATG
Tgfb1	GGA AAT CAA CGG GAT CAG CCC	GCT GCC GCA CAC AGC AGT TC
Ubc	CCC AGT GTT ACC ACC AAG AAG	CCC CAT CAC ACC CAA GAA CA
Deposited Data		
Raw and processed scRNA-seq data	NCBI Gene Expression Omnibus	GSE229257
Processed Seurat Object	Zenodo	https://doi.org/10.5281/zenodo.7608212
Experiment Models: Organisms/Strain		
Mouse C57BL/6	InVivos	n/a
Software and Algorithms		
anndata 0.8.0	PyPI	https://pypi.org
BioRender	https://biorender.com	n/a
CellChat 1.6.1	Jin *et al.* (Jin et al., 2021)	Jin *et al.* (Jin et al., 2021)
cellrank 1.5.1	Lange *et al.* (Lange et al., 2022)	Lange *et al.* (Lange et al., 2022)
Cell Ranger 6.1.2	10X Genomics, Inc.	https://www.10xgenomics.com
clustree 0.5.0	Zappia *et al.* (Zappia & Oshlack, 2018)	Zappia *et al.* (Zappia & Oshlack, 2018)
glmGamPoi 1.8.0	Ahlmann-Eltze *et al.* (Ahlmann-Eltze & Huber, 2021)	Ahlmann-Eltze *et al.* (Ahlmann-Eltze & Huber, 2021)
miQC 1.4.0	GitHub	https://github.com/greenelab/miQC
NicheNet	Browaeys *et al.* (Browaeys et al., 2020)	Browaeys *et al.* (Browaeys et al., 2020)
numpy 1.23.5	PyPI	https://pypi.org
pandas 1.5.3	PyPI	https://pypi.org
PanglaoDB	PanglaoDB	https://panglaodb.se/markers.html
Prism 9.4.1	GraphPad Software	https://www.graphpad.com
PyCharm 2022.3.3	JetBrains	https://www.jetbrains.com
Python 3.9.16	Python Software Foundation	https://python.org
R 4.2.1	The R Foundation	https://www.r-project.org
RStudio 2022.07.2+576	Posit Software	https://posit.co
samtools 1.13	GitHub	https://github.com/samtools
scanpy 1.9.1	PyPI	https://pypi.org
scipy 1.10.0	PyPI	https://pypi.org
scDblFinder 1.10.0	Germain *et al.* (Germain et al., 2021)	Germain *et al.* (Germain et al., 2021)

sctransform 0.3.5	Choudhary *et al.* (Choudhary & Satija, 2022)	Choudhary *et al.* (Choudhary & Satija, 2022)
scvelo 0.2.5	Bergen *et al.* (Bergen et al., 2020)	Bergen *et al.* (Bergen et al., 2020)
Seurat 4.3.0	Hao *et al.* (Hao et al., 2021)	Hao *et al.* (Hao et al., 2021)
UMAP	McInnes *et al.* (McInnes et al., 2018)	https://github.com/lmcinnes/umap
velocyto.py 0.17.17	La Manno *et al.* (La Manno et al., 2018)	La Manno *et al.* (La Manno et al., 2018)
WGCNA 1.72-1	Langfelder *et al.* (Langfelder & Horvath, 2008)	Langfelder *et al.* (Langfelder & Horvath, 2008)

Key resources table

Resource availability

Lead Contact

Further information and requests for resources should be directed to and will be fulfilled by the lead contacts, Kimberly Kline, at kimberly.kline@unige.ch and Guillaume Thibault, at thibault@ntu.edu.sg.

Material Availability

This study did not generate new reagents.

Data and Code Availability

The accession number for the raw data reported in this paper is GSE229257. The processed data are available at Zenodo (*https://doi.org/10.5281/zenodo.7608212*).

Method details

Mouse wound infection model

In vivo procedures were approved by the Animal Care and Use Committee of the Biological Resource Centre (Nanyang Technological University, Singapore) in accordance with the guidelines of the Agri-Food and Veterinary Authority and the National Advisory Committee for Laboratory Animal Research of Singapore (ARF SBS/NIEA-0314). Male C57BL/6 mice were housed at the Research Support Building animal facility under pathogen-free conditions. Mice between 5-7 weeks old (22–25 g; InVivos, Singapore) were used for the wound infection model, modified from a previous study (Keogh et al., 2016). Briefly, mice were anesthetized with 3% isoflurane. Dorsal hair was removed by shaving, followed by hair removal cream (Nair cream, Church and Dwight Co) application. The shaven skin was then disinfected with 70% ethanol and a 6-mm full-thickness wound was created using a biopsy punch (Integra Miltex, New York). Two mice were infected with 10 µl of 2 x108 bacteria/ml inoculum (*Enterococcus faecalis* OG1RF strain), while the other two served as controls for uninfected wounds. All wounds were sealed with transparent dressing (Tegaderm, 3M, St Paul Minnesota). Mice were euthanized four days post-infection (4 dpi), and wounds collected immediately using a biopsy punch with minimal adjacent healthy skin were stored in Hanks 'Buffered Salt Solution (HBSS; Ca2+/Mg2+-free; Sigma Aldrich, Cat. #H4385) supplemented with 0.5% bovine serum albumin (BSA; Sigma Aldrich, Cat. #A7030).

In vitro culture and infection of bone marrow-derived macrophages

Murine bone marrow-derived macrophages (BMDMs) were isolated from bone marrow cells of 7-8 weeks old C57BL/6 male mice as described previously (Toda et al., 2021), except that BMDMs were differentiated in 100 mm non-treated square dishes (Thermo Scientific, Singapore) with supplementation of 50 ng/ml M-CSF (BioLegend, Singapore). On day 6, differentiated BMDMs were harvested by gentle cell scraping in Dulbecco's PBS (DPBS; Gibco, Singapore), and 106 BMDMs were seeded in 6-well plates using bone marrow growth medium without antibiotics. Following overnight incubation, the growth medium was replaced with complete DMEM (DMEM supplemented with 10% FBS) for *E. faecalis* infection. Log-phase *E. faecalis* OG1RF cultures were washed and normalized to an OD600/ml of 0.5 in complete DMEM, equivalent to approximately 3 x 10^8 CFU/ml. BMDMs were then infected with OG1RF at a multiplicity of infection (MOI) of 10 for 1 h, followed by centrifugation at 1,000 x *g* for 5 min prior to incubation to promote BMDM-bacteria

contact. For uninfected controls, complete DMEM was added instead of MOI 10 bacterial suspension. At 1 hpi, BMDM were washed thrice with DPBS and incubated in complete DMEM supplemented with 10 µg/ml vancomycin and 150 µg/ml gentamicin for 23 h to kill extracellular bacteria, until a final time point of 24 hpi.

Quantitative qPCR analysis

Total mRNA was extracted using the TRIzol reagent (Invitrogen, cat. # 15596018) and purified using an EZ-10 DNAaway RNA Mini-Preps Kit (Bio Basic, cat. #BS88136-250). Complementary DNA (cDNA) was synthesized from total RNA using RevertAid Reverse Transcriptase (Thermo Fisher, Waltham, MA, cat. # 01327685) according to the manufacturer's protocol. Real-time PCR was performed using Luna SYBR Green (New England Biolabs, UK) according to the manufacturer's protocol using a CFX-96 Real-time PCR system (Bio-Rad, Hercules, CA, USA). A 100-ng of cDNA and 0.25 µM of the paired primer mix for target genes were used for each reaction. Relative mRNA was normalized to the housekeeping gene glyceraldehyde-3-phosphate dehydrogenase (*Gapdh*) or a geometric mean of Ct values from beta-actin (*Actb*) and ubiquitin (*Ubc*) housekeeping genes, as calculated by BestKeeper (Pfaffl et al., 2004) and log2 fold changes were plotted with reference to the uninfected, unwounded skin. The primer pairs used in this study are listed in the Key Resources Table.

Dissociation of tissue and library preparation

Tissues were transferred to a sterile 10 mm2 tissue culture dish and cut into small fragments using a sterile blade. The dissociation cocktail [10 mg/ml of dispase II (GIBCO, Cat. #17105041), 250 mg/ml of collagenase type I (GIBCO, cat. #17100017), and 2.5 mg/ml of liberase TM (Roche, cat. #5401119001)] was dissolved in HBSS. The tissue was digested enzymatically in pre-warmed dissociation buffer for 2 h at 37°C with manual orbital shaking every 15 min and then the dissociated cells were sifted through a sterile 70-µm cell strainer (Corning, cat. #352350) on ice and washed thrice with HBSS supplemented with 0.04% BSA. The remaining undigested tissue on the filter was re-incubated in 0.05%w/v trypsin/EDTA (GIBCO, cat. #25-051-CI) for 15 min at 37°C. Trypsin-digested cells were pooled with cells on ice by sifting through a sterile 70-µm cell strainer. The pooled cell suspension was washed thrice with HBSS supplemented with 0.04% BSA, followed by final filtering using a sterile 40-µm cell strainer (Corning, cat. #352340). The cell suspensions were centrifuged at 300 x *g* for 10 min, and the pellets were resuspended in Dulbecco's phosphate-buffered saline (DPBS; Thermo Fisher Scientific, cat. #14190094). Cell viability was determined by using Countess 3 FL Automated Cell Counter (Invitrogen) by mixing cell suspension with 0.4% trypan blue stain (Invitrogen, cat. #T10282) at a ratio of 1:1 for a minimum of four counts per sample. Isolated cells were encapsulated for single-cell RNA sequencing with microfluidic partitioning using the Chromium Single Cell 3' Reagent Kits (v3.1 Chemistry Dual Index, Protocol #CG000315), targeting 8,000 cells (10X Genomics, Pleasanton, CA). Libraries then were pooled by condition and sequenced on the HiSeq6000 system by NovogeneAIT (Singapore). A detailed protocol can be found at protocols.io (dx.doi.org/10.17504/protocols.io.yxmvmn8m9g3p/v1).

Data Processing

Raw data (.bcl) was used as an input to *Cell Ranger* (v6.1.2, 10X Genomics) with *mkfastq* function for trimming, base calling, and demultiplexing of reads by NovogeneAIT (Singapore). FASTQ files were aligned, filtered, barcoded and UMI counted using cellranger count command using *GENCODE vM23/Ensembl 98* (*https://cf.10xgenomics.com/supp/cell-exp/refdata-gex-GRCh38-2020-A.tar.gz*) mouse reference genome with --expect cells of 8,000 per sample on the National Supercomputer Centre Singapore (NSCC) High Power Computing platform (ASPIRE 1). The raw data can be found at Gene Expression Omnibus with the accession number GSE229257.

Integration and downstream analysis

Datasets from each sample were integrated using *Seurat* version 4.3.0 (Hao et al., 2021) on *R* (v4.2.1) using *RStudio* interface (RStudio 2022.07.2+576 "Spotted Wakerobin" release) on macOS Ventura (13.0.1). Briefly, Seurat objects were created based on the criteria of a minimum of 3 cells expressing a minimum of 200 features. Low-quality cells were determined by a probabilistic approach using the *miQC* package (v1.4.0). Similarly, doublets were removed with *scDblFinder* v1.10.0 (Germain et al., 2021). Cell cycle stages were determined by using *Seurat*'s built-in updated cell-cycle gene list. Feature counts were normalized using SCTransform() v2 regularization (Choudhary & Satija, 2022) with a scaling factor of 1x104 and Gamma-Poisson Generalized Linear Model by glmGamPoi() function (Ahlmann-Eltze & Huber, 2021), during which cell cycles and mitochondrial genes were regressed out for integration of 3,000 anchors. Fourteen principal components (PC) were included in dimension reduction calculated by the point where the change of percentage of variation was more than 0.1% between the two consecutive PCs. First, *k*-Nearest Neighbors were computed using *pca* reduction, followed by identifying original Louvain clusters with a resolution of 0.7 calculated by *clustree* v0.5.0 (Zappia & Oshlack, 2018). Uniform Manifold Approximation and Projection (UMAP) was used for visualization throughout the study (McInnes et al., 2018). A log 2-fold-change of 0.5 was set to identify gene expression markers for all clusters with min.pct of 0.25. Density plots were generated in the *Nebulosa* (v1.6.0) package to demonstrate specific cell population signatures. Finally, we computed weighted gene co-expression networks for describing the correlation patterns among genes across samples (Langfelder & Horvath, 2008). We also compared the 2D UMAP representations of the two conditions. Using the integrated dataset, we split the dataset based on the conditions by the built-in SplitObject() function of the Seurat package. Then, we computed a cross-entropy test for the UMAP projections by applying a two-sided Kolmogorov-Smirnov test (Roca et al., 2023).

Cell type annotation

An unbiased cell annotation was conducted at two levels using the *ScType* algorithm with slight modifications (Ianevski et al., 2022). First, we identified mega classes using gene set signatures on PanglaoDB (*https://panglaodb.se/*; Acc. date August 2022). Secondly, we further detailed each cluster based on published comprehensive mouse skin datasets (Joost et al., 2020; Joost et al., 2016). The processed Seurat object can be found at Zenodo (*https://doi.org/10.5281/zenodo.7608212*).

Cell-cell interactions

NicheNet's differential *R* implementation (v1.1.1) was used to interrogate cell-cell interactions (Browaeys et al., 2020). Three databases provided, namely *ligand-target prior model*, *ligand-receptor network*, and *weighted integrated networks*, were used *NicheNet*'s *Seurat* wrapper where endothelial cells were set as the receiver (receptor) cell population, and keratinocytes, fibroblasts, and macrophages were defined as the sender (ligand) populations. The *NicheNet* heat map was plotted to visualize the ligand activity-target cell gene expression matrix. We further compared cell-cell interactions between different niches to better predict niche-specific ligand-receptor (L-R) pairs using differential *NicheNet* analysis. *CellChat* (v1.6.1) was used to further identify secreted ligand-receptor pairs across all cell populations (Jin et al., 2021).

RNA velocity analysis

BAM files generated during the alignment of the raw data in Cell Ranger, were sorted by cell barcodes with sort -t CB using *samtools* (v1.13) in the command line. Spliced and unspliced reads were annotated in *velocyto.py* (v0.17.17) pipeline (La Manno et al., 2018), with repeats mask annotation file downloaded from *https://genome.ucsc.edu/* for mouse reference genome to generate .loom files. To solve full transcriptomics dynamics, we used the generalized dynamic model on *scVelo* v0.2.0 (Bergen et al., 2020) in *Python* 3 (v3.9.16) virtual environment set up in

PyCharm (Education License v2022.3.3, build PY-223.8836.43; JetBrains, Czechia), and visualized main cell populations and subset analysis with velocity stream plots and individual genes that drive RNA velocity. Lineage driving genes were computed in *CellRank* v1.5.1 (Lange et al., 2022). Annotated data (anndata) files for each cell population and condition can be found at *https://doi.org/10.5281/zenodo.7608772*. The R scripts and complete *Jupyter* notebooks are also available at *https://github.com/cenk-celik/Celik_et_al*.

Statistical analysis

Statistical analyses were performed in *R*, python and Prism 9 (v9.4.1, GraphPad) whichever was applicable for the type of analysis. *P* values were adjusted with the Benjamini-Hochberg method for high-dimensional data analysis. The details of the significance and type of the test were indicated in the figure legends. Data are expressed as median ± SEM. A p-value of 0.05 was set as a significance threshold unless stated otherwise.

Acknowledgements

We are grateful to Drs. Claudia Stocks and Sophie Janssens for helpful discussions and critical reading of the manuscript. We thank the Singapore Centre for Environmental Life Sciences Engineering High Throughput Sequencing Unit for providing us with the Chromium Controller (10X Genomics) microfluidic partitioning instrument for single-cell encapsulation. The computational work for this article was partially performed on resources of the National Supercomputing Centre (NSCC), Singapore. This work was supported by funds from the National Medical Research Council Open Fund (MOH-000566 to K.A.K. and G.T. and MOH-000645 to K.A.K.), the Singapore Ministry of Education Academic Research Fund Tier 2 (MOE2019-T2-2-089 to K.A.K.), NTU Research Scholarship to S.Y.T.L. (predoctoral fellowship), and Nanyang President's Graduate Scholarship to F.R.T. Parts of this work were also supported by the National Research Foundation and Ministry of Education Singapore under its Research Centre of Excellence Program (SCELSE).

Author contributions

Conceptualization, C.C., K.A.K. and G.T.; Methodology, C.C., F.R.T., K.A.K. and G.T.; Software, C.C.; Validation, C.C.; Formal Analysis, C.C. and F.R.T.; Investigation, C.C., S.Y.T.L., F.R.T., and M.V.; Resources, C.C. and M.V., Data Curation, C.C.; Writing – Original Draft; C.C., K.A.K., and G.T.; Writing – Review & Editing, S.Y.T.L., F.R.T, K.A.K., and G.T.; Visualization, C.C. and G.T.; Supervision, K.A.K. and G.T.; Project Administration, K.A.K. and G.T.; Funding Acquisition, K.A.K. and G.T.

Declaration of interests

The authors declare no competing financial interests.

Additional files

Table S1. Number of cells in each Louvain cluster grouped by condition. Related to **Figure 1**.

Table S2. Differential expression table of genes for the main class clusters. Related to **Figure 1C**.

Table S3. Differential expression table of genes for the main uninfected class clusters. Related to **Figure 1C**.

Table S4. Differential expression table of genes for the main infected class clusters. Related to **Figure 1C**.

Table S5. Differential expression table of genes for sub-clustered keratinocytes. Related to **Figure 2**.

Table S6. CellChat comparison for ligand:receptor pairs for the uninfected and infected datasets. Related to **Figures 2**-**6**.

Table S7. Differential expression table of genes for sub-clustered fibroblasts. Related to **Figure 3**.

Table S8. Differential expression table of genes for sub-clustered myeloid clusters. Related to **Figure 4**.

Table S9. Differential expression table of genes for sub-clustered neutrophil clusters. Related to **Figure 5**.

Supplemental information

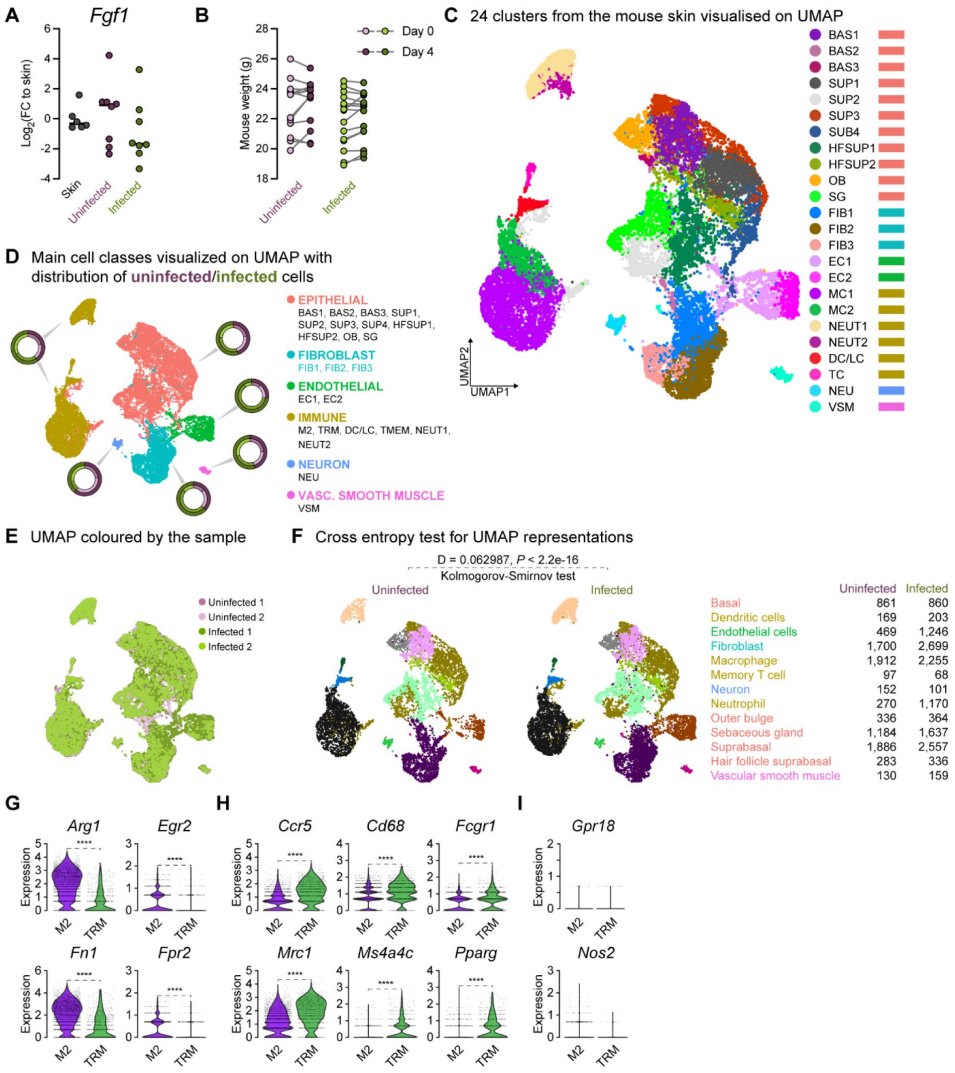

Figure S1.

Comparison of 4dpi characteristics between uninfected and E. faecalis infected in vivo and scRNA-seq data.

(A) Gene expression of fibroblast growth factor 1 (*Fgf1*) four days post-infection (4dpi) for uninfected and *E. faecalis*-infected 6–7-week-old C57BL/6J mouse skin wounds, normalized to homeostatic skin (n = 6 for skin; n = 8 for wounds; one-way ANOVA). **(B)** Weight of mice from wounding (Day 0) until 4 dpi. **(C-D)** Integrated Louvain clustering of ~23,000 scRNA-seq libraries from uninfected and infected wounds identifies 24 clusters (C) in 5 mega clusters (D), where colored circles show the contribution to the individual clusters for each condition. **(E)** UMAP colored by the sample, where shades of purple and green represent uninfected and infected conditions, respectively. **(F)** Cross entropy test for UMAP representations of uninfected and infected single-cell datasets (P value < 2.2 x 10-16, two-sided Kolmogorov-Smirnov test). **(G-I)** Comparisons of M2-like macrophage polarization (M2) markers *Arg1*, *Egr2*, *Fn1* and *Fpr2* (G), tissue-resident macrophage (TRM) markers *Ccr5*, *Cd68*, *Fcgr1*, *Mrc1* (*Cd206*), *Ms4a4c*, and *Pparg* (H), and M1-like macrophage polarization markers *Grp18* and *Nos2* (*iNos*) between the two annotated macrophage clusters (I). Wilcoxon Rank Sum test, ****p < 0.0001.

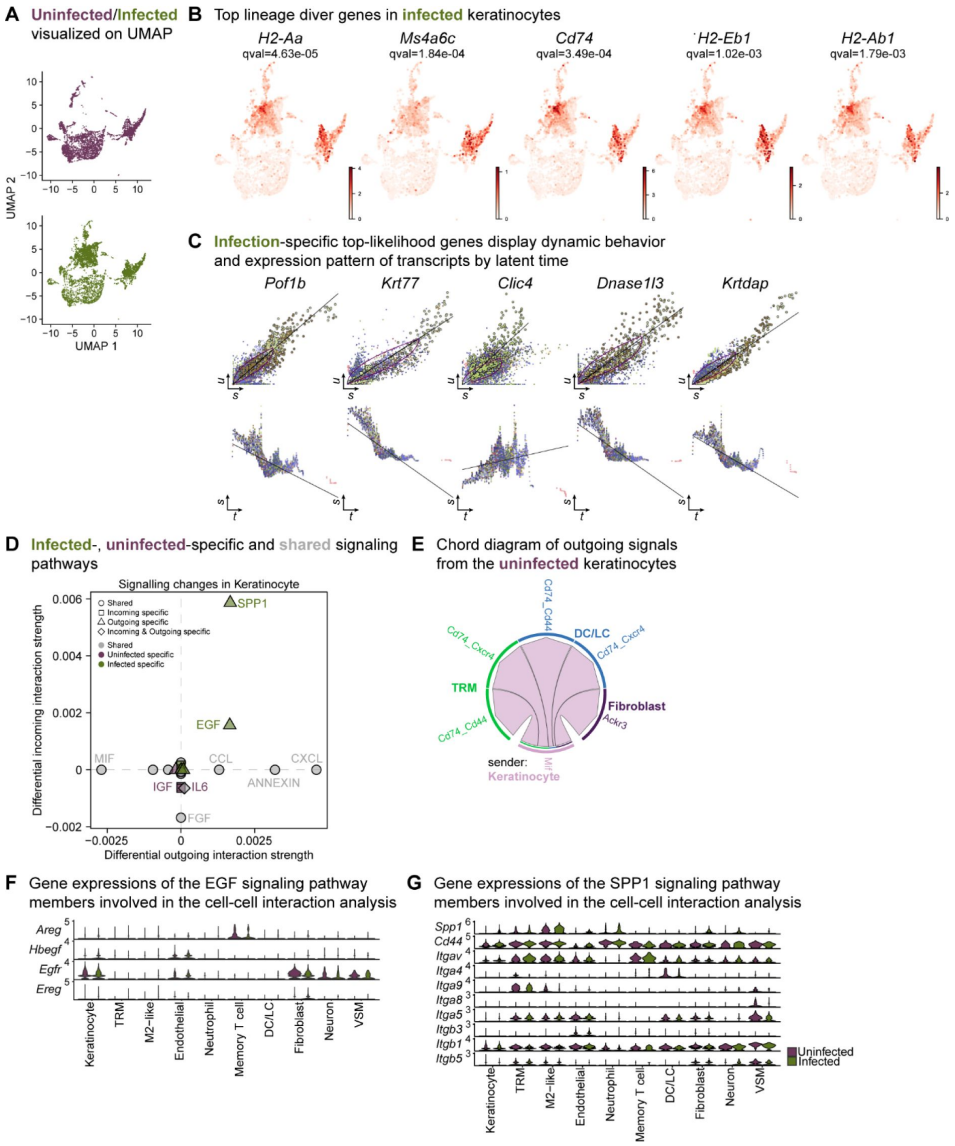

Figure S2.

Infection-specific keratinocytes display differential transcriptome.

(A) UMAP representations of the extended analysis of keratinocytes from uninfected and infected wounds. **(B)** The lineage driver genes, *H2-Aa*, *Ms4a6c*, *Cd74*, *H2-Eb1* and *H2-Ab1* in infected keratinocytes were ubiquitously expressed in infection-specific Louvain clusters. **(C)** Infection-specific top-likelihood genes display dynamic behavior (top row) and expression pattern of transcripts by latent time (bottom row). Axes denote *u* for unspliced; *s* for spliced; *t* for latent time. **(D)** Infected- (green), uninfected-specific (purple) and shared (grey) signaling pathways in keratinocytes inferred from CellChat. **(E)** Chord diagram of outgoing signals from the uninfected keratinocyte population. **(F-G)** Gene expression of the EGF (F) and SPP1 (G) signaling pathway members involved in the cell-cell interaction analysis.

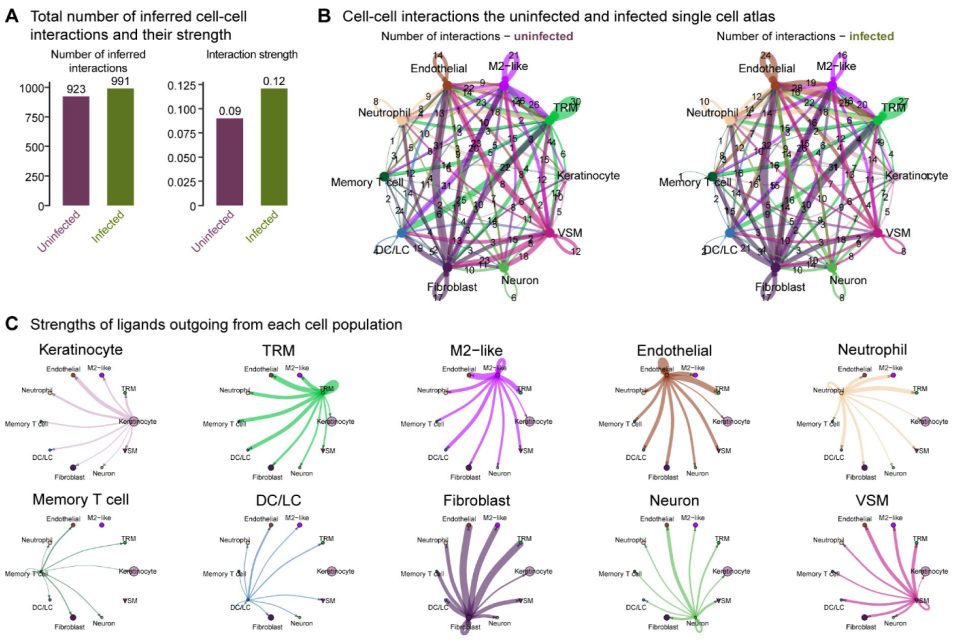

Figure S3.

Overall cellular interactome of scRNA-seq atlas.

(A) Total number of inferred cell-cell interactions and their strength computed by CellChat. **(B)** A map of cell-cell interactions in the uninfected and infected single-cell atlas, indicating the number of interactions outgoing at each node. **(C)** The strengths of ligands outgoing from each cell population.

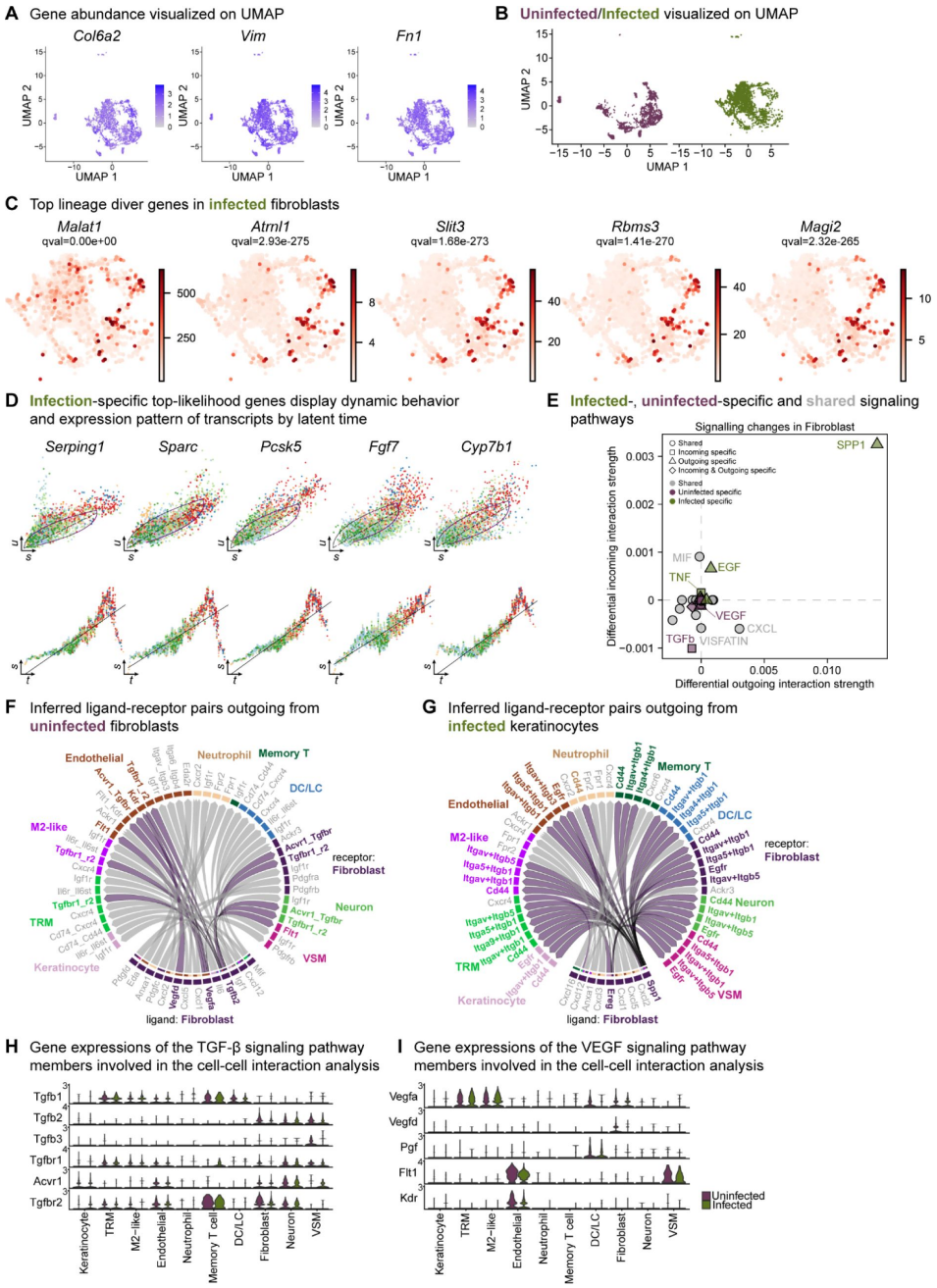

Figure S4.

Extended analysis of the fibroblast population reveals unique signatures.

(A) Spatial dispersion of fibroblast markers *Col6a2*, *Vim,* and *Fn1* in the extended analysis integrated data. **(B)** Extended analysis of fibroblasts displays infection- and healing-specific clusters. **(C)** The lineage driver genes *Malat1*, *Atrnl1*, *Slit3*, *Rbms3,* and *Magi2* were predominantly expressed in infected fibroblasts. **(D)** Infection-specific top-likelihood genes display dynamic behavior (top row) and expression pattern of transcripts by latent time (bottom row). Axes denote *u* for unspliced; *s* for spliced; *t* for latent time. **(E)** Infected-(green), uninfected-specific (purple) and shared (grey) signaling pathways in fibroblasts inferred from CellChat. **(F-G)** Chord diagram of ligand-receptor pairs in the uninfected (F) and infected (G) fibroblasts. **(I)** Inferred ligand-receptor pairs outgoing from infected fibroblasts **(H-I)** Gene expression of the TGF-β (F) and VEGF (G) signaling pathway members involved in the cell-cell interaction analysis.

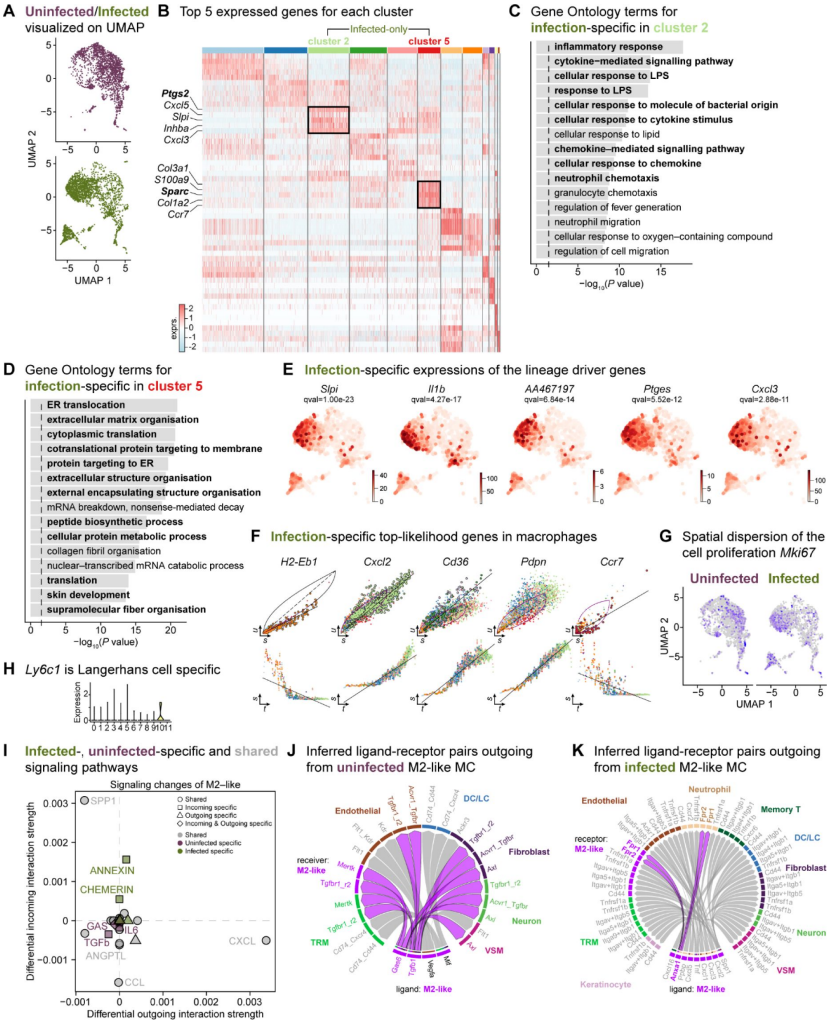

Figure S5.

The mega myeloid cell population displays M2-like polarization signatures.

(A) Split UMAP representations of the uninfected and infected myeloid cells. **(B)** Heat map of top 5 differentially expressed marker genes in macrophages. Rectangle boxes indicate infection-specific Louvain clusters. **(C-D)** The bar plots show the top 15 Gene Ontology terms for infection-specific *Ptgs2*+ (cluster 2) (C) and *Sparc*+ (cluster 5) macrophages (D). **(E)** Infection-specific expression of the lineage driver genes *Slpi*, *Il1b*, *AA467197*, *Ptges,* and *Cxcl3* indicate delayed inflammation. **(F)** Infection-specific top-likelihood genes, *Cxcl2*, *Cd36,* and *Pdpn*, were activated, while *H2-Eb1* and *Ccr7* were consumed in macrophages. **(G)** Spatial dispersion of the cell proliferation marker (*Mki67*). **(H)** Expression of *Ly6c1* was Langerhans cell-specific. **(I)** Infected-(green), uninfected-specific (purple), and shared (grey) signaling pathways in M2-like macrophages. **(J)** Chord diagram of ligand-receptor pairs in the uninfected M2-like macrophages. **(K)** Inferred ligand-receptor pairs outgoing from infected M2-like macrophages.

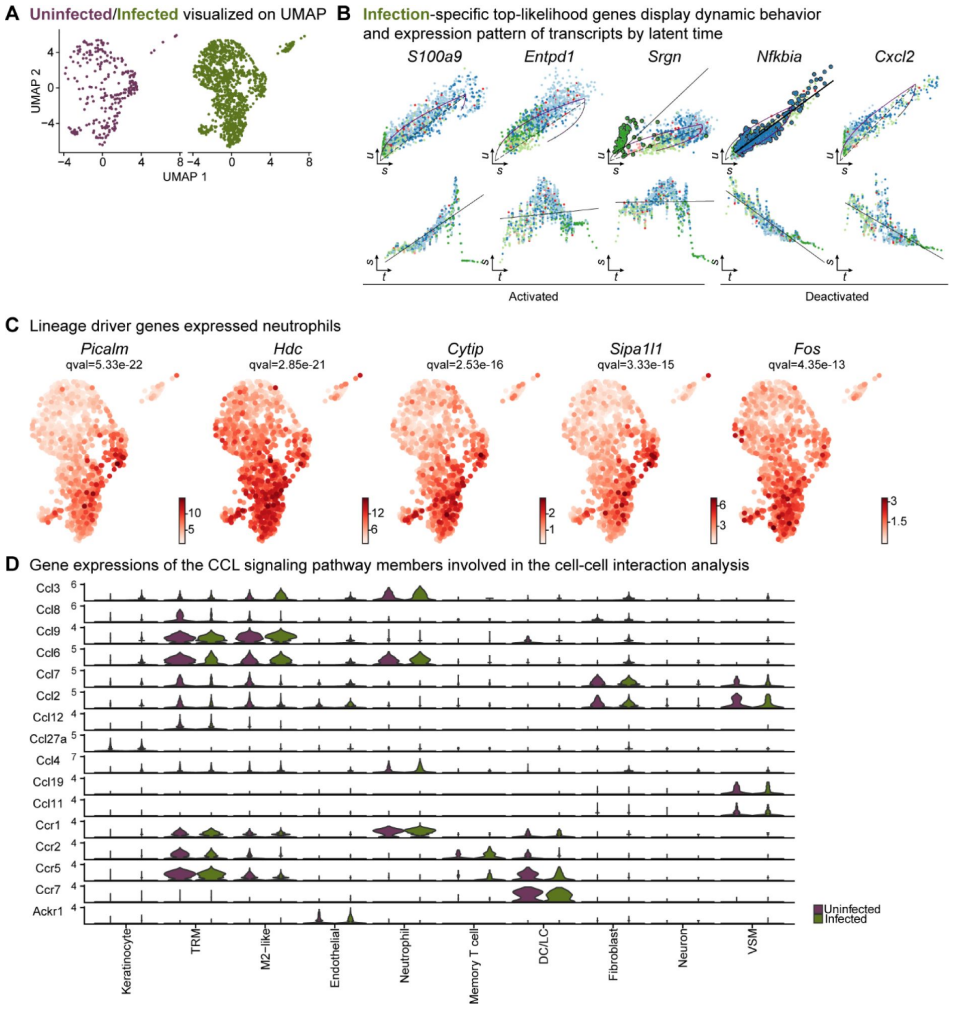

Figure S6.

Neutrophil infiltration was enhanced in response to E. faecalis infection.

(A) UMAP representations of the extended analysis of neutrophil populations in each condition. **(B)** Infection-specific top-likelihood genes display dynamic behavior (top row) and expression pattern of transcripts by latent time (bottom row). **(C)** Lineage driver genes *Picalm*, *Hdc*, *Cytip*, *Sipa1l1,* and *Fos* were highly expressed in *Lrg1hi* neutrophils. **(D)** Gene expression of the CCL signaling pathway members involved in the cell-cell interaction analysis.

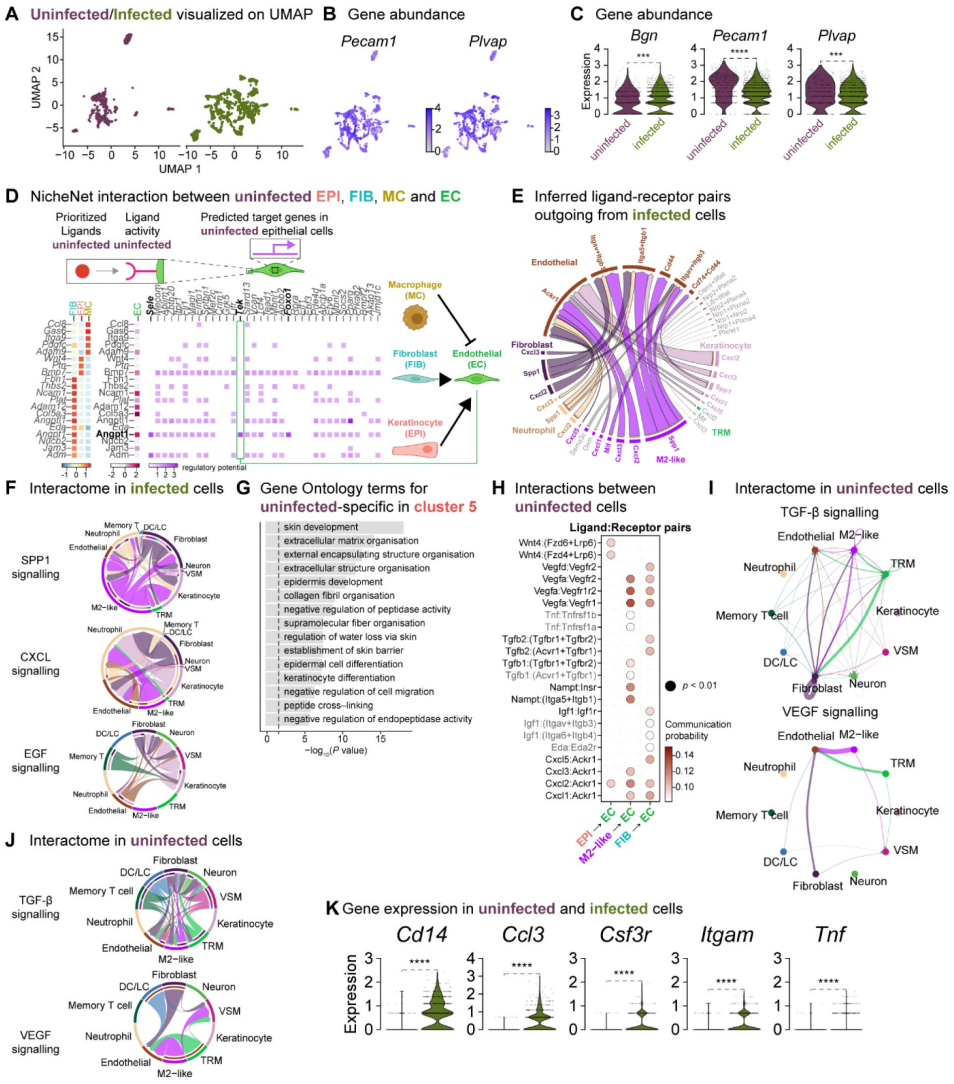

Figure S7.

Fibroblasts orchestrate a reparative niche in the uninfected wounds.

(A) UMAP representations of the uninfected and infected endothelial subsets. **(B)** Spatial dispersion of endothelial cell signatures *Pecam1* and *Plvap.* **(C)** Expressions of *Bgn*, *Pecam1,* and *Plvap* in endothelial cells (Wilcoxon Rank Sum test, **** $P <$ 0.0001, *** $P < 0.001$). **(D)** NicheNet interaction heat map between keratinocytes, fibroblasts, macrophages, and endothelial cells. Note the specific pairing of the fibroblast ligand angiopoietin 1 (*Angpt1*) with the TEK tyrosine receptor (*Tek*) in the uninfected niche. **(E)** Chord diagram of the cellular interactome between keratinocytes, fibroblasts, macrophages, and endothelial cells from infected populations. **(F)** Chord diagrams of the cellular interactome for TNF, SPP1 and CXCL signaling pathways across all cell types in infection. **(G)** Gene Ontology analysis of the uninfected specific ECs. **(H)** Dot plot of ligand:receptor pairs in the healing niche. **(I)** Differential interaction strengths of the cellular interactome for TGF-β and VEGF signaling pathways in the unwounded niche. **(J)** Chord diagrams of the cellular interactome for TGF-β and VEGF signaling pathways in the uninfected niche. **(K)** Infection-specific expression of *Cd14*, *Ccl3*, *Csf3r*, *Itgam,* and *Tnf* in endothelial cells (Wilcoxon Rank Sum test, **** $P < 0.0001$).

References

Ahlmann-Eltze C., Huber W (2021) **glmGamPoi: fitting Gamma-Poisson generalized linear models on single cell count data** *Bioinformatics* **36**:5701–5702 https://doi.org/10.1093/bioinformatics/btaa1009

Alshetaiwi H. *et al.* (2020) **Defining the emergence of myeloid-derived suppressor cells in breast cancer using single-cell transcriptomics** *Sci Immunol* **5** https://doi.org/10.1126/sciimmunol.aay6017

Ashcroft K. J., Syed F., Bayat A (2013) **Site-specific keloid fibroblasts alter the behaviour of normal skin and normal scar fibroblasts through paracrine signalling** *PLoS One* **8** https://doi.org/10.1371/journal.pone.0075600

Bao Y., Sakinc T., Laverde D., Wobser D., Benachour A., Theilacker C., Hartke A., Huebner J (2012) **Role of mprF1 and mprF2 in the pathogenicity of Enterococcus faecalis** *PLoS One* **7** https://doi.org/10.1371/journal.pone.0038458

Bergen V., Lange M., Peidli S., Wolf F. A., Theis F. J (2020) **Generalizing RNA velocity to transient cell states through dynamical modeling** *Nat Biotechnol* **38**:1408–1414 https://doi.org/10.1038/s41587-020-0591-3

Bertuccini L., Ammendolia M. G., Superti F., Baldassarri L (2002) **Invasion of HeLa cells by Enterococcus faecalis clinical isolates** *Med Microbiol Immunol* **191**:25–31 https://doi.org/10.1007/s00430-002-0115-4

Braza M. S. *et al.* (2018) **Neutrophil derived CSF1 induces macrophage polarization and promotes transplantation tolerance** *Am J Transplant* **18**:1247–1255 https://doi.org/10.1111/ajt.14645

Browaeys R., Saelens W., Saeys Y (2020) **NicheNet: modeling intercellular communication by linking ligands to target genes** *Nat Methods* **17**:159–162 https://doi.org/10.1038/s41592-019-0667-5

Ch'ng J. H., Chong K. K. L., Lam L. N., Wong J. J., Kline K. A (2019) **Biofilm-associated infection by enterococci** *Nat Rev Microbiol* **17**:82–94 https://doi.org/10.1038/s41579-018-0107-z

Chen J. *et al.* (2023) **CREB1-driven CXCR4(hi) neutrophils promote skin inflammation in mouse models and human patients** *Nat Commun* **14** https://doi.org/10.1038/s41467-023-41484-3

Cheng J. B. *et al.* (2018) **Transcriptional Programming of Normal and Inflamed Human Epidermis at Single-Cell Resolution** *Cell Rep* **25**:871–883 https://doi.org/10.1016/j.celrep.2018.09.006

Cheng M., Liang G., Yin Z., Lin X., Sun Q., Liu Y (2023) **Immunosuppressive role of SPP1-CD44 in the tumor microenvironment of intrahepatic cholangiocarcinoma assessed by single-cell RNA sequencing** *J Cancer Res Clin Oncol* **149**:5497–5512 https://doi.org/10.1007/s00432-022-04498-w

Cheng T. Y., Wu M. S., Lin J. T., Lin M. T., Shun C. T., Hua K. T., Kuo M. L (2014) **Formyl Peptide receptor 1 expression is associated with tumor progression and survival in gastric cancer** *Anticancer Res* **34**:2223–2229

Chong K. K. L. *et al.* (2017) **Enterococcus faecalis Modulates Immune Activation and Slows Healing During Wound Infection** *J Infect Dis* **216**:1644–1654 https://doi.org/10.1093/infdis/jix541

Choudhary S., Satija R (2022) **Comparison and evaluation of statistical error models for scRNA-seq** *Genome Biol* **23** https://doi.org/10.1186/s13059-021-02584-9

Cong L., Maishi N., Annan D. A., Young M. F., Morimoto H., Morimoto M., Nam J. M., Hida Y., Hida K (2021) **Inhibition of stromal biglycan promotes normalization of the tumor microenvironment and enhances chemotherapeutic efficacy** *Breast Cancer Res* **23** https://doi.org/10.1186/s13058-021-01423-w

Cuervo H., Guerrero N. A., Carbajosa S., Beschin A., De Baetselier P., Girones N., Fresno M. (2011) **Myeloid-derived suppressor cells infiltrate the heart in acute Trypanosoma cruzi infection** *J Immunol* **187**:2656–2665 https://doi.org/10.4049/jimmunol.1002928

Cutroneo K. R (2007) **TGF-beta-induced fibrosis and SMAD signaling: oligo decoys as natural therapeutics for inhibition of tissue fibrosis and scarring** *Wound Repair Regen* **15**:S54–60 https://doi.org/10.1111/j.1524-475X.2007.00226.x

da Silva R. A. G., Tay W. H., Ho F. K., Tanoto F. R., Chong K. K. L., Choo P. Y., Ludwig A., Kline K. A. (2022) **Enterococcus faecalis alters endo-lysosomal trafficking to replicate and persist within mammalian cells** *PLoS Pathog* **18** https://doi.org/10.1371/journal.ppat.1010434

Dauphinee S. M., Karsan A (2006) **Lipopolysaccharide signaling in endothelial cells** *Lab Invest* **86**:9–22 https://doi.org/10.1038/labinvest.3700366

Deng C. C. *et al.* (2021) **Single-cell RNA-seq reveals fibroblast heterogeneity and increased mesenchymal fibroblasts in human fibrotic skin diseases** *Nat Commun* **12** https://doi.org/10.1038/s41467-021-24110-y

Denhardt D. T., Noda M., O'Regan A. W., Pavlin D., Berman J. S (2001) **Osteopontin as a means to cope with environmental insults: regulation of inflammation, tissue remodeling, and cell survival** *J Clin Invest* **107**:1055–1061 https://doi.org/10.1172/JCI12980

Der E. *et al.* (2019) **Tubular cell and keratinocyte single-cell transcriptomics applied to lupus nephritis reveal type I IFN and fibrosis relevant pathways** *Nat Immunol* **20**:915–927 https://doi.org/10.1038/s41590-019-0386-1

Du Cheyne C., Tay H., De Spiegelaere W. (2020) **The complex TIE between macrophages and angiogenesis** *Anat Histol Embryol* **49**:585–596 https://doi.org/10.1111/ahe.12518

Dunny G. M., Brown B. L., Clewell D. B (1978) **Induced cell aggregation and mating in Streptococcus faecalis: evidence for a bacterial sex pheromone** *Proc Natl Acad Sci U S A* **75**:3479–3483 https://doi.org/10.1073/pnas.75.7.3479

Eming S. A., Martin P., Tomic-Canic M (2014) **Wound repair and regeneration: mechanisms, signaling, and translation** *Sci Transl Med* **6**:265–266 https://doi.org/10.1126/scitranslmed.3009337

Evrard M. *et al.* (2018) **Developmental Analysis of Bone Marrow Neutrophils Reveals Populations Specialized in Expansion, Trafficking, and Effector Functions** *Immunity* **48**:364–379 https://doi.org/10.1016/j.immuni.2018.02.002

Fang T., Zhang L., Yin X., Wang Y., Zhang X., Bian X., Jiang X., Yang S., Xue Y (2023) **The prognostic marker elastin correlates with epithelial-mesenchymal transition and vimentin-positive fibroblasts in gastric cancer** *J Pathol Clin Res* **9**:56–72 https://doi.org/10.1002/cjp2.298

Farr L., Ghosh S., Moonah S (2020) **Role of MIF Cytokine/CD74 Receptor Pathway in Protecting Against Injury and Promoting Repair** *Front Immunol* **11** https://doi.org/10.3389/fimmu.2020.01273

Fingleton B (2017) **Matrix metalloproteinases as regulators of inflammatory processes** *Biochim Biophys Acta Mol Cell Res* https://doi.org/10.1016/j.bbamcr.2017.05.010

Fitzgerald A. A., Weiner L. M (2020) **The role of fibroblast activation protein in health and malignancy** *Cancer Metastasis Rev* **39**:783–803 https://doi.org/10.1007/s10555-020-09909-3

Franzen O., Gan L. M., Bjorkegren J. L. M (2019) **PanglaoDB: a web server for exploration of mouse and human single-cell RNA sequencing data** *Database (Oxford* **2019** https://doi.org/10.1093/database/baz046

Gao W., Liu D., Sun H., Shao Z., Shi P., Li T., Yin S., Zhu T (2022) **SPP1 is a prognostic related biomarker and correlated with tumor-infiltrating immune cells in ovarian cancer** *BMC Cancer* **22** https://doi.org/10.1186/s12885-022-10485-8

Gentry-Weeks C. R., Karkhoff-Schweizer R., Pikis A., Estay M., Keith J. M (1999) **Survival of Enterococcus faecalis in mouse peritoneal macrophages** *Infect Immun* **67**:2160–2165 https://doi.org/10.1128/IAI.67.5.2160-2165.1999

Germain P. L., Lun A., Garcia Meixide C., Macnair W., Robinson M. D (2021) **Doublet identification in single-cell sequencing data using scDblFinder** *F1000Res* **10** https://doi.org/10.12688/f1000research.73600.2

Girbl T. *et al.* (2018) **Distinct Compartmentalization of the Chemokines CXCL1 and CXCL2 and the Atypical Receptor ACKR1 Determine Discrete Stages of Neutrophil Diapedesis** *Immunity* **49**:1062–1076 https://doi.org/10.1016/j.immuni.2018.09.018

Gornicki T., Lambrinow J., Mrozowska M., Podhorska-Okolow M., Dziegiel P., Grzegrzolka J (2022) **Role of RBMS3 Novel Potential Regulator of the EMT Phenomenon in Physiological and Pathological Processes** *Int J Mol Sci* **23** https://doi.org/10.3390/ijms231810875

Guasch G., Schober M., Pasolli H. A., Conn E. B., Polak L., Fuchs E (2007) **Loss of TGFbeta signaling destabilizes homeostasis and promotes squamous cell carcinomas in stratified epithelia** *Cancer Cell* **12**:313–327 https://doi.org/10.1016/j.ccr.2007.08.020

Guerrero-Juarez C. F. *et al.* (2019) **Single-cell analysis reveals fibroblast heterogeneity and myeloid-derived adipocyte progenitors in murine skin wounds** *Nat Commun* **10** https://doi.org/10.1038/s41467-018-08247-x

Haensel D. *et al.* (2020) **Defining Epidermal Basal Cell States during Skin Homeostasis and Wound Healing Using Single-Cell Transcriptomics** *Cell Rep* **30**:3932–3947 https://doi.org/10.1016/j.celrep.2020.02.091

Hao Y. *et al.* (2021) **Integrated analysis of multimodal single-cell data** *Cell* **184**:3573–3587 https://doi.org/10.1016/j.cell.2021.04.048

Hautz T. *et al.* (2023) **Immune cell dynamics deconvoluted by single-cell RNA sequencing in normothermic machine perfusion of the liver** *Nat Commun* **14** https://doi.org/10.1038/s41467-023-37674-8

Hofer F., Di Sario G., Musiu C., Sartoris S., De Sanctis F., Ugel S. (2021) **A Complex Metabolic Network Confers Immunosuppressive Functions to Myeloid-Derived Suppressor Cells (MDSCs) within the Tumour Microenvironment** *Cells* **10** https://doi.org/10.3390/cells10102700

Horsley H., Dharmasena D., Malone-Lee J., Rohn J. L (2018) **A urine-dependent human urothelial organoid offers a potential alternative to rodent models of infection** *Sci Rep* **8** https://doi.org/10.1038/s41598-018-19690-7

Horsley H., Malone-Lee J., Holland D., Tuz M., Hibbert A., Kelsey M., Kupelian A., Rohn J. L (2013) **Enterococcus faecalis subverts and invades the host urothelium in patients with chronic urinary tract infection** *PLoS One* **8** https://doi.org/10.1371/journal.pone.0083637

Hu J. *et al.* (2020) **Macrophage-derived SPARC Attenuates M2-mediated Pro-tumour Phenotypes** *J Cancer* **11**:2981–2992 https://doi.org/10.7150/jca.39651

Ianevski A., Giri A. K., Aittokallio T (2022) **Fully-automated and ultra-fast cell-type identification using specific marker combinations from single-cell transcriptomic data** *Nat Commun* **13** https://doi.org/10.1038/s41467-022-28803-w

Jager B., Klatt D., Plappert L., Golpon H., Lienenklaus S., Barbosa P. D., Schambach A., Prasse A (2020) **CXCR4/MIF axis amplifies tumor growth and epithelial-mesenchymal interaction in non-small cell lung cancer** *Cell Signal* **73** https://doi.org/10.1016/j.cellsig.2020.109672

Jin S., Guerrero-Juarez C. F., Zhang L., Chang I., Ramos R., Kuan C. H., Myung P., Plikus M. V., Nie Q (2021) **Inference and analysis of cell-cell communication using CellChat** *Nat Commun* **12** https://doi.org/10.1038/s41467-021-21246-9

Joost S., Annusver K., Jacob T., Sun X., Dalessandri T., Sivan U., Sequeira I., Sandberg R., Kasper M (2020) **The Molecular Anatomy of Mouse Skin during Hair Growth and Rest** *Cell Stem Cell* **26**:441–457 https://doi.org/10.1016/j.stem.2020.01.012

Joost S., Jacob T., Sun X., Annusver K., La Manno G., Sur I., Kasper M. (2018) **Single-Cell Transcriptomics of Traced Epidermal and Hair Follicle Stem Cells Reveals Rapid Adaptations during Wound Healing** *Cell Rep* **25**:585–597 https://doi.org/10.1016/j.celrep.2018.09.059

Joost S., Zeisel A., Jacob T., Sun X., La Manno G., Lonnerberg P., Linnarsson S., Kasper M. (2016) **Single-Cell Transcriptomics Reveals that Differentiation and Spatial Signatures Shape Epidermal and Hair Follicle Heterogeneity** *Cell Syst* **3**:221–237 https://doi.org/10.1016/j.cels.2016.08.010

Kandaswamy K. *et al.* (2013) **Focal targeting by human beta-defensin 2 disrupts localized virulence factor assembly sites in Enterococcus faecalis** *Proc Natl Acad Sci U S A* **110**:20230–20235 https://doi.org/10.1073/pnas.1319066110

Kao P. H., Ch'ng J. H., Chong K. K. L., Stocks C. J., Wong S. L., Kline K. A (2023) **Enterococcus faecalis suppresses Staphylococcus aureus-induced NETosis and promotes bacterial survival in polymicrobial infections** *FEMS Microbes* **4** https://doi.org/10.1093/femsmc/xtad019

Kao P. H. N., Kline K. A (2019) **Dr. Jekyll and Mr. Hide: How Enterococcus faecalis Subverts the Host Immune Response to Cause Infection** . *J Mol Biol* **431**:2932–2945 https://doi.org/10.1016/j.jmb.2019.05.030

Keogh D., Tay W. H., Ho Y. Y., Dale J. L., Chen S., Umashankar S., Williams R. B. H., Chen S. L., Dunny G. M., Kline K. A (2016) **Enterococcal Metabolite Cues Facilitate Interspecies Niche Modulation and Polymicrobial Infection** *Cell Host Microbe* **20**:493–503 https://doi.org/10.1016/j.chom.2016.09.004

Kim S. Y., Nair M. G (2019) **Macrophages in wound healing: activation and plasticity** *Immunol Cell Biol* **97**:258–267 https://doi.org/10.1111/imcb.12236

Krzyszczyk P., Schloss R., Palmer A., Berthiaume F (2018) **The Role of Macrophages in Acute and Chronic Wound Healing and Interventions to Promote Pro-wound Healing Phenotypes** *Front Physiol* **9** https://doi.org/10.3389/fphys.2018.00419

La Manno G. *et al.* (2018) **RNA velocity of single cells** *Nature* **560**:494–498 https://doi.org/10.1038/s41586-018-0414-6

Landen N. X., Li D., Stahle M (2016) **Transition from inflammation to proliferation: a critical step during wound healing** *Cell Mol Life Sci* **73**:3861–3885 https://doi.org/10.1007/s00018-016-2268-0

Lange M. *et al.* (2022) **CellRank for directed single-cell fate mapping** *Nat Methods* **19**:159–170 https://doi.org/10.1038/s41592-021-01346-6

Langfelder P., Horvath S (2008) **WGCNA: an R package for weighted correlation network analysis** *BMC Bioinformatics* **9** https://doi.org/10.1186/1471-2105-9-559

Li X. *et al.* (2021) **Pinocembrin Ameliorates Skin Fibrosis via Inhibiting TGF-beta1 Signaling Pathway** *Biomolecules* **11** https://doi.org/10.3390/biom11081240

Lindley L. E., Stojadinovic O., Pastar I., Tomic-Canic M (2016) **Biology and Biomarkers for Wound Healing** *Plast Reconstr Surg* https://doi.org/10.1097/PRS.0000000000002682

Lloyd K. L., Kubes P (2006) **GPI-linked endothelial CD14 contributes to the detection of LPS** *Am J Physiol Heart Circ Physiol* **291**:H473–481 https://doi.org/10.1152/ajpheart.01234.2005

Maloney J., Keselman A., Li E., Singer S. M (2015) **Macrophages expressing arginase 1 and nitric oxide synthase 2 accumulate in the small intestine during Giardia lamblia infection** *Microbes Infect* **17**:462–467 https://doi.org/10.1016/j.micinf.2015.03.006

Masson-Meyers D. S., Andrade T. A. M., Caetano G. F., Guimaraes F. R., Leite M. N., Leite S. N., Frade M. A. C (2020) **Experimental models and methods for cutaneous wound healing assessment** *Int J Exp Pathol* **101**:21–37 https://doi.org/10.1111/iep.12346

Mattila J. T. *et al.* (2013) **Microenvironments in tuberculous granulomas are delineated by distinct populations of macrophage subsets and expression of nitric oxide synthase and arginase isoforms** *J Immunol* **191**:773–784 https://doi.org/10.4049/jimmunol.1300113

McInnes L., Healy J., Melville J (2018) **Umap: Uniform manifold approximation and projection for dimension reduction** *arXiv preprint arXiv*

Meister M. *et al.* (2015) **Self-Antigen Presentation by Keratinocytes in the Inflamed Adult Skin Modulates T-Cell Auto-Reactivity** *J Invest Dermatol* **135**:1996–2004 https://doi.org/10.1038/jid.2015.130

Minutti C. M., Knipper J. A., Allen J. E., Zaiss D. M (2017) **Tissue-specific contribution of macrophages to wound healing** *Semin Cell Dev Biol* **61**:3–11 https://doi.org/10.1016/j.semcdb.2016.08.006

Mizumoto S. *et al.* (2020) **CSGALNACT1-congenital disorder of glycosylation: A mild skeletal dysplasia with advanced bone age** *Hum Mutat* **41**:655–667 https://doi.org/10.1002/humu.23952

Morimoto H., Hida Y., Maishi N., Nishihara H., Hatanaka Y., Li C., Matsuno Y., Nakamura T., Hirano S., Hida K (2021) **Biglycan, tumor endothelial cell secreting proteoglycan, as possible biomarker for lung cancer** *Thorac Cancer* **12**:1347–1357 https://doi.org/10.1111/1759-7714.13907

Munadziroh E., Askandar M. G., Yuliati A., Surboyo M. D. C., Wan Harun W. H. A (2022) **The effect of secretory leukocyte protease inhibitor amnion membrane on incisional wound healing** *J Oral Biol Craniofac Res* **12**:358–362 https://doi.org/10.1016/j.jobcr.2022.04.001

Na Y. R., Yoon Y. N., Son D. I., Seok S. H (2013) **Cyclooxygenase-2 inhibition blocks M2 macrophage differentiation and suppresses metastasis in murine breast cancer model** *PLoS One* **8** https://doi.org/10.1371/journal.pone.0063451

Nunez N., Derre-Bobillot A., Trainel N., Lakisic G., Lecomte A., Mercier-Nome F., Cassard A. M., Bierne H., Serror P., Archambaud C (2022) **The unforeseen intracellular lifestyle of Enterococcus faecalis in hepatocytes** *Gut Microbes* **14** https://doi.org/10.1080/19490976.2022.2058851

Olmsted S. B., Dunny G. M., Erlandsen S. L., Wells C. L (1994) **A plasmid-encoded surface protein on Enterococcus faecalis augments its internalization by cultured intestinal epithelial cells** *J Infect Dis* **170**:1549–1556 https://doi.org/10.1093/infdis/170.6.1549

Orecchioni M., Ghosheh Y., Pramod A. B., Ley K (2019) **Macrophage Polarization: Different Gene Signatures in M1(LPS+) vs. Classically and M2(LPS-) vs. Alternatively Activated Macrophages** *Front Immunol* **10** https://doi.org/10.3389/fimmu.2019.01084

Pakyari M., Farrokhi A., Maharlooei M. K., Ghahary A (2013) **Critical Role of Transforming Growth Factor Beta in Different Phases of Wound Healing** *Adv Wound Care (New Rochelle)* **2**:215–224 https://doi.org/10.1089/wound.2012.0406

Perrault D. P., Bramos A., Xu X., Shi S., Wong A. K (2018) **Local Administration of Interleukin-1 Receptor Antagonist Improves Diabetic Wound Healing** *Ann Plast Surg* **80** https://doi.org/10.1097/SAP.0000000000001417

Pfaffl M. W., Tichopad A., Prgomet C., Neuvians T. P (2004) **Determination of stable housekeeping genes, differentially regulated target genes and sample integrity: BestKeeper--Excel-based tool using pair-wise correlations** *Biotechnol Lett* **26**:509–515 https://doi.org/10.1023/b:bile.0000019559.84305.47

Philippeos C. *et al.* (2018) **Spatial and Single-Cell Transcriptional Profiling Identifies Functionally Distinct Human Dermal Fibroblast Subpopulations** *J Invest Dermatol* **138**:811–825 https://doi.org/10.1016/j.jid.2018.01.016

Rashid R. *et al.* (2023) **Depleting Cationic Lipids Involved in Antimicrobial Resistance Drives Adaptive Lipid Remodeling in Enterococcus faecalis** *mBio* **14** https://doi.org/10.1128/mbio.03073-22

Recalcati S., Gammella E., Buratti P., Doni A., Anselmo A., Locati M., Cairo G (2019) **Macrophage ferroportin is essential for stromal cell proliferation in wound healing** *Haematologica* **104**:47–58 https://doi.org/10.3324/haematol.2018.197517

Roca C. P., Burton O. T., Neumann J., Tareen S., Whyte C. E., Gergelits V., Veiga R. V., Humblet-Baron S., Liston A (2023) **A cross entropy test allows quantitative statistical comparison of t-SNE and UMAP representations** *Cell Rep Methods* **3** https://doi.org/10.1016/j.crmeth.2022.100390

Rognoni E., Watt F. M (2018) **Skin Cell Heterogeneity in Development, Wound Healing, and Cancer** *Trends Cell Biol* **28**:709–722 https://doi.org/10.1016/j.tcb.2018.05.002

Sawant K. V., Sepuru K. M., Lowry E., Penaranda B., Frevert C. W., Garofalo R. P., Rajarathnam K (2021) **Neutrophil recruitment by chemokines Cxcl1/KC and Cxcl2/MIP2: Role of Cxcr2 activation and glycosaminoglycan interactions** *J Leukoc Biol* **109**:777–791 https://doi.org/10.1002/JLB.3A0820-207R

Schultz G., Rotatori D. S., Clark W (1991) **EGF and TGF-alpha in wound healing and repair** *J Cell Biochem* **45**:346–352 https://doi.org/10.1002/jcb.240450407

Siriwach R., Ngo A. Q., Narumiya S., Thumkeo D (2022) **An optimized protocol to identify keratinocyte subpopulations in vitro by single-cell RNA sequencing analysis** *STAR Protoc* **3** https://doi.org/10.1016/j.xpro.2022.101906

Standal T., Borset M., Sundan A (2004) **Role of osteopontin in adhesion, migration, cell survival and bone remodeling** *Exp Oncol* **26**:179–184

Takaoka R. T. C., Sertorio N. D., Magalini L. P. J., Dos Santos L. M., Souza H. R., Iyomasa-Pilon M. M., Possebon L., Costa S. S., Girol A. P (2018) **Expression profiles of Annexin A1, formylated peptide receptors and cyclooxigenase-2 in gastroesophageal inflammations and neoplasias** *Pathol Res Pract* **214**:181–186 https://doi.org/10.1016/j.prp.2017.12.003

Tamoutounour S. *et al.* (2019) **Keratinocyte-intrinsic MHCII expression controls microbiota-induced Th1 cell responses** *Proc Natl Acad Sci U S A* **116**:23643–23652 https://doi.org/10.1073/pnas.1912432116

Tan C. A. Z., Lam L. N., Biukovic G., Soh E. Y., Toh X. W., Lemos J. A., Kline K. A (2022) **Enterococcus faecalis Antagonizes Pseudomonas aeruginosa Growth in Mixed-Species Interactions** *J Bacteriol* **204** https://doi.org/10.1128/jb.00615-21

Theocharidis G. *et al.* (2022) **Murine macrophages or their secretome delivered in alginate dressings enhance impaired wound healing in diabetic mice** *Biomaterials* **288** https://doi.org/10.1016/j.biomaterials.2022.121692

Tien B. Y. Q., Goh H. M. S., Chong K. K. L., Bhaduri-Tagore S., Holec S., Dress R., Ginhoux F., Ingersoll M. A., Williams R. B. H., Kline K. A (2017) **Enterococcus faecalis Promotes Innate Immune Suppression and Polymicrobial Catheter-Associated Urinary Tract Infection** *Infect Immun* **85** https://doi.org/10.1128/IAI.00378-17

Toda G., Yamauchi T., Kadowaki T., Ueki K (2021) **Preparation and culture of bone marrow-derived macrophages from mice for functional analysis** *STAR Protoc* **2** https://doi.org/10.1016/j.xpro.2020.100246

Vecchi L. *et al.* (2018) **Inhibition of the AnxA1/FPR1 autocrine axis reduces MDA-MB-231 breast cancer cell growth and aggressiveness in vitro and in vivo** *Biochim Biophys Acta Mol Cell Res* **1865**:1368–1382 https://doi.org/10.1016/j.bbamcr.2018.06.010

Veglia F., Sanseviero E., Gabrilovich D. I (2021) **Myeloid-derived suppressor cells in the era of increasing myeloid cell diversity** *Nat Rev Immunol* **21**:485–498 https://doi.org/10.1038/s41577-020-00490-y

Vu R., Jin S., Sun P., Haensel D., Nguyen Q. H., Dragan M., Kessenbrock K., Nie Q., Dai X (2022) **Wound healing in aged skin exhibits systems-level alterations in cellular composition and cell-cell communication** *Cell Rep* **40** https://doi.org/10.1016/j.celrep.2022.111155

Wang M., Chaudhuri R., Ong W. W. S., Sintim H. O (2021) **c-di-GMP Induces COX-2 Expression in Macrophages in a STING-Independent Manner** *ACS Chem Biol* **16**:1663–1670 https://doi.org/10.1021/acschembio.1c00342

Wang P. H., Huang B. S., Horng H. C., Yeh C. C., Chen Y. J (2018) **Wound healing** *J Chin Med Assoc* **81**:94–101 https://doi.org/10.1016/j.jcma.2017.11.002

Watanabe S., Alexander M., Misharin A. V., Budinger G. R. S (2019) **The role of macrophages in the resolution of inflammation** *J Clin Invest* **129**:2619–2628 https://doi.org/10.1172/JCI124615

Wells C. L., Jechorek R. P., Erlandsen S. L (1990) **Evidence for the translocation of Enterococcus faecalis across the mouse intestinal tract** *J Infect Dis* **162**:82–90 https://doi.org/10.1093/infdis/162.1.82

Wells C. L., Jechorek R. P., Maddaus M. A., Simmons R. L (1988) **Effects of clindamycin and metronidazole on the intestinal colonization and translocation of enterococci in mice** *Antimicrob Agents Chemother* **32**:1769–1775 https://doi.org/10.1128/AAC.32.12.1769

Wilkinson H. N., Hardman M. J (2020) **Wound healing: cellular mechanisms and pathological outcomes** *Open Biol* **10** https://doi.org/10.1098/rsob.200223

Xie Y., Gao K., Hakkinen L., Larjava H. S (2009) **Mice lacking beta6 integrin in skin show accelerated wound repair in dexamethasone impaired wound healing model** *Wound Repair Regen* **17**:326–339 https://doi.org/10.1111/j.1524-475X.2009.00480.x

Yang Y. H., Aeberli D., Dacumos A., Xue J. R., Morand E. F (2009) **Annexin-1 regulates macrophage IL-6 and TNF via glucocorticoid-induced leucine zipper** *J Immunol* **183**:1435–1445 https://doi.org/10.4049/jimmunol.0804000

Zappia L., Oshlack A (2018) **Clustering trees: a visualization for evaluating clusterings at multiple resolutions** *Gigascience* **7** https://doi.org/10.1093/gigascience/giy083

Zhao L., Wang W., Niu P., Luan X., Zhao D., Chen Y (2022) **The molecular mechanisms of CTHRC1 in gastric cancer by integrating TCGA, GEO and GSA datasets** *Front Genet* **13** https://doi.org/10.3389/fgene.2022.900124

Zou J., Shankar N (2014) **Enterococcus faecalis infection activates phosphatidylinositol 3-kinase signaling to block apoptotic cell death in macrophages** *Infect Immun* **82**:5132–5142 https://doi.org/10.1128/IAI.02426-14

Zou J., Shankar N (2016) **The opportunistic pathogen Enterococcus faecalis resists phagosome acidification and autophagy to promote intracellular survival in macrophages** *Cell Microbiol* **18**:831–843 https://doi.org/10.1111/cmi.12556

Article and author information

Cenk Celik
School of Biological Sciences, Nanyang Technological University, Singapore
ORCID iD: 0000-0001-8301-0172

Stella Yue Ting Lee
School of Biological Sciences, Nanyang Technological University, Singapore
ORCID iD: 0000-0003-3475-7709

Frederick Reinhart Tanoto
Singapore Centre for Environmental Life Science Engineering, Nanyang Technological University, Singapore
ORCID iD: 0000-0001-9289-4811

Mark Veleba
Singapore Centre for Environmental Life Science Engineering, Nanyang Technological University, Singapore
ORCID iD: 0000-0002-9516-8660

Kimberly A. Kline
School of Biological Sciences, Nanyang Technological University, Singapore, Singapore Centre for Environmental Life Science Engineering, Nanyang Technological University, Singapore, Department of Microbiology and Molecular Medicine, Faculty of Medicine, University of Geneva, Switzerland
For correspondence: Kimberly.Kline@unige.ch
ORCID iD: 0000-0002-5472-3074

Guillaume Thibault
School of Biological Sciences, Nanyang Technological University, Singapore, Mechanobiology Institute, National University of Singapore, Singapore
For correspondence: thibault@ntu.edu.sg
ORCID iD: 0000-0002-7926-4812

Copyright

Editors

Reviewing Editor
Russell Vance
University of California, Berkeley, Berkeley, United States of America

Senior Editor
Satyajit Rath
Indian Institute of Science Education and Research (IISER), Pune, India

Reviewer #1 (Public Review):

Summary:

This is an interesting study that performs scRNA-Seq on infected and uninfected wounds. The authors sought to understand how infection with E. faecalis influences the transcriptional profile of healing wounds. The analysis demonstrated that there is a unique transcriptional profile in infected wounds with specific changes in macrophages, keratinocytes, and fibroblasts. They also speculated on potential crosstalk between macrophages and neutrophils and macrophages and endothelial cells using NicheNet analysis and CellChat. Overall the data suggest that infection causes keratinocytes to not fully transition which may impede their function in wound healing and that the infection greatly influenced the transcriptional profile of macrophages and how they interact with other cells.

Strengths:

It is a useful dataset to help to understand the impact of wound infection on transcription of specific cell types. The analysis is very thorough in terms of transcriptional analysis and uses a variety of techniques and metrics.

Weaknesses:

Some drawbacks of the study are the following. First the fact that it only has two mice per group, and only looks at one time point after wounding decreases the impact of the study. Wound healing is a dynamic and variable process so understanding the full course of the wound healing response would be very important to understand the impact of infection on the healing wound. The analysis has been bolstered by applying a cross-entropy test on the integrated dataset and to ensure robustness of the datasets (Fig S1F). Including unwounded skin in the scRNA-Seq would also lend a lot more significance to this study. However, this was technically challenging due to constraints with the number of immune cells in unwounded skin as described in the limitations section. Another drawback of the study is that mouse punch biopsies are very different than human wounds as they heal primarily by contraction instead of re-epithelialization like human wounds. The authors mitigated this somewhat be extracting the incisional parts of the wound. So while the conclusions are generally supported the scope of the work is somewhat limited.

https://doi.org/10.7554/eLife.95113.2.sa1

Reviewer #2 (Public Review):

Summary:

The authors have performed a detailed analysis of the complex transcriptional status of numerous cell types present in wounded tissue, including keratinocytes, fibroblasts, macrophages, neutrophils, and endothelial cells. The comparison between infected and uninfected wounds is interesting and the analysis suggests possible explanations for why infected wounds are delayed in their healing response.

Strengths:

The paper presents a thorough and detailed analysis of the scRNAseq data. The paper is clearly written and the conclusions drawn from the analysis are appropriately cautious. The results provide an important foundation for future work on the healing of infected and uninfected wounds.

Weaknesses:

The analysis is purely descriptive and no attempt is made to validate whether any of the factors identified are playing functional roles in wound healing. Such experiments would be appropriate for followup work. The experimental setup is analyzing a single time point and does not include a comparison to unwounded skin. Nevertheless, the present data do provide a useful point of comparison for the field.

https://doi.org/10.7554/eLife.95113.2.sa0

Author response:

The following is the authors' response to the original reviews.

> ***Public Reviews:***
>
> ***Reviewer #1 (Public Review):***
>
> *Summary:*
>
> *This is an interesting study that performs scRNA-Seq on infected and uninfected wounds. The authors sought to understand how infection with E. faecalis influences the transcriptional profile of healing wounds. The analysis demonstrated that there is a unique transcriptional profile in infected wounds with specific changes in macrophages, keratinocytes, and fibroblasts. They also speculated on potential crosstalk between macrophages and neutrophils and macrophages and endothelial cells using NicheNet analysis and CellChat. Overall the data suggest that infection causes keratinocytes to not fully transition which may impede their function in wound healing and that the infection greatly influenced the transcriptional profile of macrophages and how they interact with other cells.*
>
> *Strengths:*
>
> *It is a useful dataset to help understand the impact of wound infection on the transcription of specific cell types. The analysis is very thorough in terms of transcriptional analysis and uses a variety of techniques and metrics.*
>
> *Weaknesses:*

> *Some drawbacks of the study are the following. First, the fact that it only has two mice per group, and only looks at one time point after wounding decreases the impact of the study. Wound healing is a dynamic and variable process so understanding the full course of the wound healing response would be very important to understand the impact of infection on the healing wound. Including unwounded skin in the scRNA-Seq would also lend a lot more significance to this study. Another drawback of the study is that mouse punch biopsies are very different than human wounds as they heal primarily by contraction instead of reepithelialization like human wounds. So while the conclusions are generally supported the scope of the work is limited.*

Thank you for your thoughtful review and acknowledgment of the thoroughness of our analysis.

> *First, the fact that it only has two mice per group, and only looks at one time point after wounding decreases the impact of the study.*

We acknowledge your concerns regarding the limitations of our study, particularly regarding the small number of mice per group and the examination of only one time point post-wounding. We agree that a more comprehensive analysis across multiple time points would provide a deeper understanding of the temporal changes induced by infection. While our primary focus in this study was to elucidate the foundational responses to bacteria-infected wounds, we attempted to augment our analysis by incorporating publicly available datasets of similar nature. However, these datasets lacked power in terms of cell number and populations. Nonetheless, we have bolstered our analysis by applying a crossentropy test on the integrated dataset and reporting its significance (Figure S1F), ensuring the robustness of our single-cell RNA sequencing datasets.

> *Including unwounded skin in the scRNA-Seq would also lend a lot more significance to this study.*

We also recognize the significance of comparing infected wounds to unwounded skin to establish a baseline for transcriptional changes. While we attempted to incorporate publicly available unwounded skin samples into our analysis, we encountered limitations in the number of cells, particularly within the immune population. This constraint is addressed in the Limitations section of the manuscript.

> *Another drawback of the study is that mouse punch biopsies are very different than human wounds as they heal primarily by contraction instead of re-epithelialization like human wounds.*

Regarding the concern about differences between murine and human wound healing mechanisms, we took measures during tissue isolation to mitigate this issue, extracting incisions of the wounds rather than contracted tissues. Despite the primary mode of wound closure in mice being contraction, we believe our analysis still offers valuable insights into cellular responses to infection relevant to human wound healing.

We appreciate your constructive criticism of our study. Despite these constraints, we believe our work provides valuable insights into the transcriptional changes induced by infection in healing wounds.

> ***Reviewer #2 (Public Review):***
>
> *Summary:*

> *The authors have performed a detailed analysis of the complex transcriptional status of numerous cell types present in wounded tissue, including keratinocytes, fibroblasts, macrophages, neutrophils, and endothelial cells. The comparison between infected and uninfected wounds is interesting and the analysis suggests possible explanations for why infected wounds are delayed in their healing response.*
>
> *Strengths:*
>
> *The paper presents a thorough and detailed analysis of the scRNAseq data. The paper is clearly written and the conclusions drawn from the analysis are appropriately cautious. The results provide an important foundation for future work on the healing of infected and uninfected wounds.*
>
> *Weaknesses:*
>
> *The analysis is purely descriptive and no attempt is made to validate whether any of the factors identified are playing functional roles in wound healing. The experimental setup is analyzing a single time point and does not include a comparison to unwounded skin.*

We are thankful for your acknowledgment of the thoroughness of our analysis and the cautious nature of our conclusions.

> *The analysis is purely descriptive, and no attempt is made to validate whether any of the factors identified are playing functional roles in wound healing.*

Regarding your concern about the purely descriptive nature of our analysis and the lack of functional validation of identified factors, we agree on the importance of understanding the functional roles of transcriptional changes in wound healing. To address this limitation, we plan to conduct functional experiments, such as perturbation assays or in vivo validation studies, to validate the roles of specific factors identified in our analysis.

> *The experimental setup is analyzing a single time point and does not include a comparison to unwounded skin.*

We acknowledge the importance of comparing wounded tissue to unwounded skin to establish a baseline for understanding transcriptional changes. This point is noted and acknowledged in the limitations section of our manuscript.

We appreciate your feedback and assure you that we will consider your suggestions in future iterations of our research.

We are grateful for the positive overall assessment of our revised work by the reviewers. Critical comments on specific aspects of our work are listed verbatim below followed by our responses.

> ***Reviewer 1 (Recommendations for the Authors):***
>
> *(1) The figures are a bit cluttered and hard to parse out. The different parts of the figure seem to be scattered all over the place with no consistent order.*

Thank you for your feedback regarding the figures in our manuscript. We acknowledge your concern that some panels may appear cluttered and challenging to navigate. In response, we

> ***Recommendations For The Authors:***

We are grateful for the positive overall assessment of our revised work by the reviewers. Critical comments on specific aspects of our work are listed verbatim below followed by our responses.

> ***Reviewer 1 (Recommendations for the Authors):***
>
> *(1) The figures are a bit cluttered and hard to parse out. The different parts of the figure seem to be scattered all over the place with no consistent order.*

Thank you for your feedback regarding the figures in our manuscript. We acknowledge your concern that some panels may appear cluttered and challenging to navigate. In response, we made concerted efforts to declutter certain panels, taking into account page size constraints and ensuring a minimum font size for readability.

> *(2) I didn't really understand what the last sentence on page 6 meant. Is this meant to say that these could be biomarkers of infection?*

We thank the reviewer for noting this lack of clarity. We revised the statement.

Updated manuscript (lines 111-113)

“Overall, the persistent E. faecalis infection contributed to higher Tgfb1 expression, whilst Pdgfa levels remained low, correlating with delayed wound healing.”

> *(3) >(3) A reference on page 19 didn't format correctly.*

We thank the reviewer for catching the typos. We corrected the reference formatting.

Updated manuscript (lines 503-505)

“We confirm the immune-suppressive role of E. faecalis in wound healing, consistent with previous findings in different experimental settings (Chong et al., 2017; Kao et al., 2023; Tien et al., 2017).”

> *(4) The title doesn't really address the scope of the finding which goes beyond immunomodulatory.*

The reviewer is correct! We therefore revised the title to cover all aspects of the study as:

“Decoding the complexity of delayed wound healing following Enterococcus faecalis infection”

> ***Reviewer 2 (Recommendations for the Authors):***
>
> *(1) On page 6, the expression of Tgfb1 is described as "aggravated" by wounding alone. I am not sure whether this means Tgfb1 levels are increased or decreased. It appears from the data that it is increased, which was confusing to me since I interpreted "aggravated" as meaning decreased. So perhaps a different more straightforward word could be used to describe the data.*

We modified this ambiguous statement to:

Updated manuscript (lines 105-106)

“By contrast, wounding alone resulted in higher transforming growth factor beta 1 (Tgfb1) expression.”

> *(2) On page 7, the authors state that "cells from infected wounds…demonstrated distinct clustering patterns compared to cells from uninfected wounds (Figure S1F)" but when I look at the data in this figure, I cannot really see a difference. Perhaps the differences could be more clearly highlighted?*

Thank you for pointing out this issue. We appreciate the reviewer's comment. We utilized the crossentropy test for statistical comparison, employing UMAP embedding space data. While the data underwent batch correction based on infection status, the UMAP plots for each condition may appear visually similar. However, it's important to note that the number of cells per clusters between the infected and uninfected conditions varies significantly. This aspect influences the selection of points (cells) and their nearest neighbours for statistical testing within each cluster in the embedding space. To address this concern, we have included a table indicating the number of cells per cell type alongside the plot (Figure S1F), providing additional context for the interpretation of our results.

Author response table 1.

	Uninfected	Infected
Basal	861	860
Dendritic cells	169	203
Endothelial cells	469	1,246
Fibroblast	1,700	2,699
Macrophage	1,912	2,255
Memory T cell	97	68
Neuron	152	101
Neutrophil	270	1,170
Outer bulge	336	364
Sebaceous gland	1,184	1,637
Suprabasal	1,886	2,557
Hair follicle suprabasal	283	336
Vascular smooth muscle	130	159

Author response image 1.

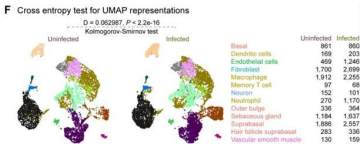

> *(3) On page 8, Zeb2hi cells are described as "immunosuppressive" and yet the genes are highlighted to express in include Cxcl2 and IL1b which I would classify as inflammatory, not immunosuppressive. Can the authors be a bit more clear on why they describe the phenotype of these cells as "immunosuppressive"?*

We agree with the reviewer that this is a bit counterintuitive. Conventionally, CXCL2 is thought to be chemoattractant for neutrophil recruitment. However, the infection-specific keratinocyte cluster expressing Cxcl2, Il1b, Wfdc17 along with Zeb2 and Thbs1 indicate their myeloid-derived suppressor cell-like features, which play immunosuppressive roles during infection and in cancer (Alshetaiwi et al., 2020; Siriwach et al., 2022; Veglia et al., 2021).

Updated manuscript (lines 159-163)

“As the barrier to pathogens, keratinocytes secrete a broad range of cytokines that can induce inflammatory responses (Alshetaiwi et al., 2020; Siriwach et al., 2022; Veglia et al., 2021). However, Zeb2hi keratinocytes co-expressing Cxcl2, Il1b, and Wfdc17, indicate myeloidderived suppressor cell-like phenotype which implies an immunosuppressive environment (Hofer et al., 2021; Veglia et al., 2021).”

> *(4) On pages 8-9, Keratinocytes are described to express MHC class II. I find this quite unexpected since class II is usually thought to be expressed primarily by APCs such as DCs and B cells. Is there a precedent for keratinocytes to express class II? The authors should acknowledge that this is unexpected and in need of further validation, or support the claim with references in which class II expression has been previously observed on keratinocytes (and is thus not unexpected)*

Although MHC class II expression is predominantly on immune cells, an antigen-presenting role for keratinocytes has been reported in many studies (Banerjee et al., 2004; Black et al., 2007; Carr et al., 1986; Gawkrodger et al., 1987; Jiang et al., 2020; Li et al., 2022; Oh et al., 2019; Tamoutounour et al., 2019). Therefore, antigen-presenting role of keratinocytes is known and expected, and we think that this should be further investigated in in the context of wound infection.

Updated manuscript (lines 177-179)

"These genes are associated with the major histocompatibility complex (MHC) class II, suggesting a self-antigen presenting keratinocyte population, which have a role in costimulation of T cell responses (Meister et al., 2015; Tamoutounour et al., 2019)."

REFERENCES

Alshetaiwi, H., Pervolarakis, N., McIntyre, L. L., Ma, D., Nguyen, Q., Rath, J. A., Nee, K., Hernandez, G., Evans, K., Torosian, L., Silva, A., Walsh, C., & Kessenbrock, K. (2020). Defining the emergence of myeloid-derived suppressor cells in breast cancer using single-cell transcriptomics. Science Immunology, 5(44), eaay6017. https://doi.org/10.1126/sciimmunol.aay6017

Banerjee, G., Damodaran, A., Devi, N., Dharmalingam, K., & Raman, G. (2004). Role of keratinocytes in antigen presentation and polarization of human T lymphocytes. Scandinavian Journal of Immunology, 59(4), 385–394. https://doi.org/10.1111/j.0300-9475.2004.01394.x

Black, A. P. B., Ardern-Jones, M. R., Kasprowicz, V., Bowness, P., Jones, L., Bailey, A. S., & Ogg, G. S. (2007). Human keratinocyte induction of rapid effector function in antigen-specific memory CD4+ and CD8+ T cells. European Journal of Immunology, 37(6), 1485–1493. https://doi.org/10.1002/eji.200636915

Carr, M. M., McVittie, E., Guy, K., Gawkrodger, D. J., & Hunter, J. A. (1986). MHC class II antigen expression in normal human epidermis. Immunology, 59(2), 223–227.

Gawkrodger, D. J., Carr, M. M., McVittie, E., Guy, K., & Hunter, J. A. (1987). Keratinocyte expression of MHC class II antigens in allergic sensitization and challenge reactions and in irritant contact dermatitis. The Journal of Investigative Dermatology, 88(1), 11–16. https://doi.org/10.1111/1523-1747.ep12464641

Jiang, Y., Tsoi, L. C., Billi, A. C., Ward, N. L., Harms, P. W., Zeng, C., Maverakis, E., Kahlenberg, J. M., & Gudjonsson, J. E. (2020). Cytokinocytes: The diverse contribution of keratinocytes to immune responses in skin. JCI Insight, 5(20), e142067, 142067. https://doi.org/10.1172/jci.insight.142067

Li, D., Cheng, S., Pei, Y., Sommar, P., Kärner, J., Herter, E. K., Toma, M. A., Zhang, L., Pham, K., Cheung, Y. T., Liu, Z., Chen, X., Eidsmo, L., Deng, Q., & Xu Landén, N. (2022). Single-Cell Analysis Reveals Major Histocompatibility Complex II–Expressing Keratinocytes in Pressure Ulcers with Worse Healing Outcomes. The Journal of Investigative Dermatology, 142(3 Pt A), 705–716. https://doi.org/10.1016/j.jid.2021.07.176

Oh, S., Chung, H., Chang, S., Lee, S.-H., Seok, S. H., & Lee, H. (2019). Effect of Mechanical Stretch on the DNCB-induced Proinflammatory Cytokine Secretion in Human Keratinocytes. Scientific Reports, 9(1), 5156. https://doi.org/10.1038/s41598-019-41480-y

Siriwach, R., Ngo, A. Q., Higuchi, M., Arima, K., Sakamoto, S., Watanabe, A., Narumiya, S., & Thumkeo, D. (2022). Single-cell RNA sequencing identifies a migratory keratinocyte subpopulation expressing THBS1 in epidermal wound healing. iScience, 25(4), 104130. https://doi.org/10.1016/j.isci.2022.104130

Tamoutounour, S., Han, S.-J., Deckers, J., Constantinides, M. G., Hurabielle, C., Harrison, O. J., Bouladoux, N., Linehan, J. L., Link, V. M., Vujkovic-Cvijin, I., Perez-Chaparro, P. J., Rosshart, S. P., Rehermann, B., Lazarevic, V., & Belkaid, Y. (2019). Keratinocyte-intrinsic MHCII expression controls microbiota-induced Th1 cell responses. Proceedings of the National Academy of Sciences of the United States of America, 116(47), 23643–23652. https://doi.org/10.1073/pnas.1912432116

Veglia, F., Sanseviero, E., & Gabrilovich, D. I. (2021). Myeloid-derived suppressor cells in the era of increasing myeloid cell diversity. Nature Reviews. Immunology, 21(8), 485–498. https://doi.org/10.1038/s41577-020-00490-y